VOL.107 NO.HY8. AUG. 1981

JOURNAL OF THE HYDRAULICS DIVISION

PROCEEDINGS OF
THE AMERICAN SOCIETY
OF CIVIL ENGINEERS

VOL.107 NO.HY8. AUG. 1981

JOURNAL OF THE HYDRAULICS DIVISION

PROCEEDINGS OF
THE AMERICAN SOCIETY
OF CIVIL ENGINEERS

Copyright© 1981 by
American Society
of Civil Engineers
All Rights Reserved
ISSN 0044-796X

Melvin W. Anderson, Editor
University of South Florida

AMERICAN SOCIETY OF CIVIL ENGINEERS

BOARD OF DIRECTION

President
Irvan F. Mendenhall

Past President
Joseph S. Ward

President Elect
James R. Sims

Vice Presidents
Robert D. Bay — Lyman R. Gillis
Francis J. Connell — Albert A. Grant

Directors
Martin G. Abegg — Paul R. Munger
Floyd A. Bishop — William R. Neuman
L. Gary Byrd — Leonard S. Oberman
Larry J. Feeser — John D. Parkhurst
John A. Focht, Jr. — Celestino R. Pennoni
Sergio Gonzalez-Karg — Robert B. Rhode
James E. Humphrey, Jr. — S. Russell Stearns
Richard W. Karn — William H. Taylor
Leon D. Luck — Stafford E. Thornton
Arthur R. McDaniel — Robert E. Whiteside
Richard S. Woodruff

EXECUTIVE OFFICERS

Eugene Zwoyer, *Executive Director*
Julie E. Gibouleau, *Assistant to the Executive Director*
Louis L. Meier, *Washington Counsel/Assistant Secretary*
William H. Wisely, *Executive Director Emeritus*
Michael N. Salgo, *Treasurer*
Elmer B. Isaak, *Assistant Treasurer*

STAFF DIRECTORS

Donald A. Buzzell, *Managing Director for Education and Professional Affairs*
Robert A. Crist, Jr., *Managing Director for Publications and Technical Affairs*
Alexandra Bellow, *Director, Human Resources*
David Dresia, *Director, Publications Production and Marketing*
Barker D. Herr, *Director, Membership*
Richard A. Jeffers, *Controller*
Carl E. Nelson, *Director, Field Services*
Don P. Reynolds, *Director, Policy, Planning and Public Affairs*
Bruce Rickerson, *Director, Legislative Services*
Albert W. Turchick, *Director, Technical Services*
George K. Wadlin, *Director, Education Services*
R. Lawrence Whipple, *Director, Engineering Management Services*

COMMITTEE ON PUBLICATIONS

Stafford E. Thornton, *Chairman*
Martin G. Abegg — Richard W. Karn
John A. Focht, Jr. — Paul R. Munger
William R. Neuman

HYDRAULICS DIVISION

Executive Committee
Ronald E. Nece, *Chairman*
Rudolph P. Savage, *Vice Chairman*
George E. Hecker — Ralph M. Weaver
Charles S. Mifkovic, *Secretary*
John J. Cassidy, *Management Group D Contact Member*

Publications Committee
Melvin W. Anderson, ***Chairman and Editor***
John A. Hoopes, ***Vice Chairman***
Philip H. Burgi, *Hydraulic Structures*
Richard H. (Pete) Hawkins, *Surface Water Hydrology*
John A. Hoopes, *Hydromechanics, General*
Gerhard H. Jirka, *Hydraulic Transport and Dispersion*
Chintu Lai, *Hydromechanics, Open Channels*
Frederick A. Locher, *Hydromechanics, Open Channels*
Donn G. DeCoursey, *Sedimentation*
Bryan R. Pearce, *Tidal Hydraulics*
John A. Roberson, *Hydromechanics, Closed Conduits*
John L. Wilson, *Groundwater Hydrology*
George E. Hecker, *Exec. Comm. Contact Member*

PUBLICATION SERVICES DEPARTMENT

David Dresia, *Director, Publications Production and Marketing*

Technical and Professional Publications

Richard R. Torrens, *Manager*
Chuck Wahrhaftig, *Chief Copy Editor*
Corinne Bernstein, *Copy Editor*
Linda Ellington, *Copy Editor*
Shiela Menaker, *Production Co-ordinator*
Richard C. Scheblein, *Draftsman*

Information Services

Elan Garonzik, *Editor*

PERMISSION TO PHOTOCOPY JOURNAL PAPERS

Permission to photocopy for personal or internal reference beyond the limits in Sections 107 and 108 of the U.S. Copyright Law is granted by the American Society of Civil Engineers for libraries and other users registered with the Copyright Clearance Center, 21 Congress Street, Salem, Mass. 01970, provided the appropriate fee is paid to the CCC for all articles bearing the CCC code. Requests for special permission or bulk copying should be addressed to the Manager of Technical and Professional Publications, American Society of Civil Engineers.

CONTENTS

Two Bed-Load Formulas: An Evaluation
by Magdy I. Amin and Peter J. Murphy 961

Vertical Velocity Profiles in Stratified Flows
by Steve C. McCutcheon 973

Turbulence Model for Flow over Dredged Channels
by C. Koutitas and B. O'Connor 989

Water Routing on Diverging-Converging Watersheds
by Necati Ağiralioğlu 1003

The Journal of the Hydraulics Division (ISSN 0044-796X) is published monthly by the American Society of Civil Engineers. Publications office is at 345 East 47th Street, New York, N.Y. 10017. Address all ASCE correspondence to the Editorial and General Offices at 345 East 47th Street, New York, N.Y. 10017. Allow six weeks for change of address to become effective. Subscription price to members is $16.50. Nonmember subscriptions available; prices obtainable on request. Second-class postage paid at New York, N.Y. and at additional mailing offices. HY.

POSTMASTER: Send address changes to American Society of Civil Engineers, 345 East 47th Street, New York, NY 10017.

The Society is not responsible for any statement made or opinion expressed in its publications.

DISCUSSION

Proc. Paper 16409

Bayesian Frequency Analysis,[a] by Wilson H. Tang (July, 1980).
by Arun Kumar and Rema Devi 1021
by Donthamsetti V. Rao 1023

Improved Stability of Dronkers' Tidal Schemes,[a] by Guss S. Stelling (Aug., 1980).
errata 1025

Geometry of Gravel Streams,[a] by Howard H. Chang (Sept., 1980).
by Timothy R. H. Davies 1026

Minimum Stream Power: Theory,[a] by Charles C. S. Song and Chih Ted Yang (Sept., 1980).
by Timothy R. H. Davies 1026

INFORMATION RETRIEVAL

The key words, abstract, and reference "cards" for each article in this Journal represent part of the ASCE participation in the EJC information retrieval plan. The retrieval data are placed herein so that each can be cut out, placed on a 3 × 5 card and given an accession number for the user's file. The accession number is then entered on key word cards so that the user can subsequently match key words to choose the articles he wishes. Details of this program were given in an August, 1962 article in CIVIL ENGINEERING, reprints of which are available on request to ASCE headquarters.

[a]Discussion period closed for this paper. Any other discussion received during this discussion period will be published in subsequent Journals.

16448 TWO BED-LOAD FORMULAS: AN EVALUATION

KEY WORDS: **Bed load;** Beds under water; **Channel beds;** Channels (waterways); **Comparative studies; Formulas (mathematics);** Instrumentation; River beds; **Sands;** Sediments; **Sediment transport**

ABSTRACT: An evaluation of formulas is presented for the prediction of bed load in sand-bottomed channels. The evaluation is done by measuring both the hydraulic data needed for the formulas and the actual sediment transport rate, and comparing the predicted with the observed values. The results indicate that the Toffaleti procedure predicts the transport rate with sufficient accuracy to be useful for most engineering purposes.

REFERENCE: Amin, Magdy I. (Lect., Dept. of Civ. Engrg., Ain Shams Univ., Cairo, Egypt), and Murphy, Peter J., "Two Bed-Load Formulas: An Evaluation," *Journal of the Hydraulics Division,* ASCE, Vol. 107, No. HY8, **Proc. Paper 16448**, August, 1981, pp. 961-972

16422 PROFILES IN STRATIFIED FLOWS

KEY WORDS: **Density;** Fluid mechanics; **Open channel flow;** Saline water; **Stratification; Turbulent flow; Velocity;** Velocity measurement

ABSTRACT: The Monin-Obukhov analysis is applied to stably stratified, two-dimensional, hydraulically rough, turbulent, fully developed, open-channel flows. The buoyancy flux is expressed as a function of the velocity and density gradients for cases in which the buoyancy flux may vary over the depth. Resulting vertical velocity profile expressions were verified with experimental data collected in a wide laboratory flume with salt-stratified flows. Sidewall effects on stratified flows are significant in narrow flumes and are magnified in highly stratified flows, as noted in a review of previous works.

REFERENCE: McCutcheon, Steve C. (Hydrologist, U.S. Geological Survey, Gulf Coast Hydroscience Center, NSTL Station, Miss., 39529), "Vertical Velocity Profiles in Stratified Flows," *Journal of the Hydraulics Division,* ASCE, Vol. 107, No. HY8, **Proc. Paper 16422**, August, 1981, pp. 973-988

16449 MODEL FOR FLOW OVER DREDGED CHANNELS

KEY WORDS: **Approach channels; Channels (waterways);** Computation; Computer models; **Dredging;** Eddies; Estuaries; **Flow patterns;** Mathematical models; Nonuniform flow; **Turbulence**

ABSTRACT: The mathematical model of nearly horizontal flows is applied for the study of the nonuniform flow over a steep-sided, dredged, port approach channel. A mixed finite-difference/finite-element method is used for the solution. The eddy viscosity parameter is computed by means of both the mixing length and turbulence kinetic energy turbulence closures. The comparison of the computed flow magnitudes (velocity, eddy viscosity, shear stresses, and turbulence kinetic energy) to the laboratory measured ones demonstrate the predictive character of the model.

REFERENCE: Koutitas, C. (Lect., Hydraulics Dept., School of Tech., Thessaloniki Univ., Thessaloniki, Greece), and O'Connor, B., "Turbulence Model for Flow over Dredged Channels," *Journal of the Hydraulics Division,* ASCE, Vol. 107, No. HY8, **Proc. Paper 16449**, August, 1981, pp. 989-1002

16454 ROUTING ON DIVERGING-CONVERGING WATERSHEDS

KEY WORDS: Conversion; Diversion; Floods; **Mathematical models; Overland flow;** Rainfall; Rainfall-runoff relationships; **Surface dynamics;** Surface runoff; **Watersheds; Wave equations**

ABSTRACT: For a diverging-converging surface, the kinematic wave equations are solved using an implicit finite difference method. This diverging-converging representation is applicable to a natural watershed that has a leaf-shaped geometry. The results are compared with other idealistic representations. These are: plane surface, diverging surface, and converging surface. The diverging-converging model gives hydrograph values between those of converging and diverging models, depending on the geometric parameters. In general, the geometry of a watershed has important effects on the runoff hydrograph for both equilibrium and partial equilibrium conditions.

REFERENCE: Agiralioglu, Necati (Asst. Prof. of Civ. Engrg., Technical Univ. of Istanbul, Istanbul, Turkey), "Water Routing on Diverging-Converging Watersheds," *Journal of the Hydraulics Division,* ASCE, Vol. 107, No. HY8, **Proc. Paper 16454,** August, 1981, pp. 1003-1017

TWO BED-LOAD FORMULAS: AN EVALUATION

By Magdy I. Amin,[1] and Peter J. Murphy,[2] A. M. ASCE

INTRODUCTION

There are many formulas for the prediction of the rate of sediment transport in rivers. However, the predictions do not agree with one another, and so they do not define the transport rate in a satisfactory way. This problem was considered by Vanoni (9) and Shen (7), and state-of-the-art recommendations were made. The focus of this paper is the evaluation of two of these predictive formulas when they are applied to sand-bottomed channels. The formulas selected for study were chosen both for their perceived importance and to correspond to the limitations of the measurement procedure. The first writer (1) has reported the evaluation of 10 equations. The best two of the 10, the Meyer-Peter and Müller formula (5) and the Toffaleti formula (8), will be treated herein.

Most of the sediment discharge formulas predict bed-load discharge, because bed load is logically dependent on the local properties of the channel. The prediction of suspended sediment transport is more difficult since the transport at any cross section depends on the balance between the particles going into suspension and the deposition from suspension over a long upstream reach. Therefore, bed-load formulas were chosen.

The evaluation is done by measuring both the hydraulic data needed for the formulas and also the actual sediment transport rate, and then comparing the predicted with the observed values. The bed-load formulas use the local mean velocity, flow rate, bed shear stress, or stream power to predict the transport rate at a particular site in a river. Since the equations assume uniform steady flow, to apply them to a river channel it is necessary to find: (1) A reach of the river that is roughly straight and has a fairly uniform width and depth; and (2) a period when the flow is steady. Even under these conditions the wide variation of the depth with the distance across a cross section makes it desirable to divide the cross section into subsections, as is usually done when current-meter measurements were made. The test site was chosen to meet these conditions, and the cross section was divided into five subsections.

[1] Lect., Dept. of Civ. Engrg., Ain Shams Univ., Cairo, Egypt.
[2] Asst. Prof., Dept. of Civ. Engrg., Univ. of Massachusetts, Amherst, Mass. 01003.

Note.—Discussion open until January 1, 1982. To extend the closing date one month, a written request must be filed with the Manager of Technical and Professional Publications, ASCE. Manuscript was submitted for review for possible publication on July 22, 1980. This paper is part of the Journal of the Hydraulics Division, Proceedings of the American Society of Civil Engineers, ©ASCE, Vol. 107, No. HY8, August, 1981. ISSN 0044-796X/81/0008-0961/$01.00.

Field Test

The sediment discharge data were taken at Fish Creek, near Rome, N.Y. using the compartmented sediment trap described in detail in Ref. 6. The test site is shown in Fig. 1(*a*). It was located on one side of an island that was being formed in the center of a wide crossover of the meandering channel. The mean water-surface slope, S_m, was measured with point gages installed in the channel, 343 m apart, at cross sections of nearly equal area. The creek bed was covered with a combination of ripples and dunes in the typical manner of sand-bottomed channels. The wavelength and amplitude of the dunes were roughly 10 m and 0.3 m, respectively, while the wavelength and amplitude of the ripples were approx 0.3 m and 0.03 m. The average value of the sieve diameter, d_{50}, of the sand at the site was 0.4 mm.

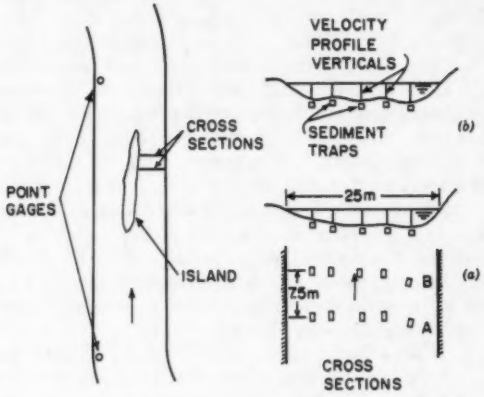

FIG. 1.—Fish Creek Field Site

Detailed flow measurements were made at two cross sections of the channel, as shown in Fig. 1(*b*). Velocity profiles were taken at the 10 verticals shown, and samples of the moving sediment were collected at the base of each vertical. The velocity was measured with a Price current meter and the sediment was caught in 10 compartmented sediment traps. The grain size of the bottom and of the samples was measured with standard sieves. The water temperature was measured with a mercury thermometer, and the duration of the sediment collection period was observed with a stopwatch.

The placement of the sediment traps in the stream bed presented some difficulty. At first, a digging tower similar to an offshore oil drilling platform was used. Its operation was so slow that only one trap could be used each day. Next, digging frames were used in shallow water where wading was possible, and this procedure was sufficiently rapid so that 10 trap samples with their corresponding velocity profiles could be obtained in a day. Finally, the digging frames were used by divers in the cold, deep, fast-flowing water of the spring runoff. That process was roughly half as fast as the wading procedure. Due to the

presence of suspended sediment, few samples were taken at these higher flow rates.

The operation of the 10 traps and the collection of the auxiliary data required four people. An outline of the procedure is presented herein. More detail is available in Ref. 1.

1. Install the digging frame in the channel bed near the middle of a dune.
2. Fill the trap with water and place the closed trap in the frame.
3. Wait until the natural state of the ripples returns to the sand bed above the trap.
4. Measure the velocity profile, $U(z)$, and depth, h, at each trap location.
5. Measure the mean channel slope, S_m, and water temperature, T.
6. Open the trap's cover and collect a sediment sample during a period of sufficient duration to gather 0.5 kg. During this period observe the trap periodically to insure proper operation. The collection period varied from 0.5 h–111.3 h.
7. Close the trap and remove it from the stream bed without spilling the sample. If the trap was open for more than 1 day, repeat the auxiliary data.
8. Dry, weigh, sieve, and reweigh the samples using standard grain size analysis techniques.

The field data were analyzed in order to calculate the hydraulic variables typically used to describe a river. The friction velocity, V_*, and the height of zero velocity, z_o, of the logarithmic velocity profile were obtained from a linear regression analysis of the velocity profile data for each trap location. The correlation coefficients were usually above 0.90 for these analyses. The mean velocity, V, was obtained from the numerical integration of velocity profile over each trap's vertical. The local bed shear stress, τ_o, was calculated from ρV_*^2, and the Darcy-Weisback friction-factor, f, was calculated from $\rho V_*^2 / V^2$. The velocity profile data were checked for accuracy by calculating the von Karmen constant, κ, from the mean velocity equation

$$\kappa = \frac{V_*}{V}\left[\ln\left(\frac{h}{z_o}\right) + \frac{z_o}{h} - 1\right] \quad \ldots\ldots\ldots\ldots\ldots\ldots\ldots\ldots\ldots\ldots (1)$$

The mean value of κ was 0.404 with a standard deviation of 0.035, indicating that the measured velocity distributions were the expected logarithmic profiles. The sediment samples collected in the containers of each trap were weighed and the spacial distribution of the sediment in the trap was checked for accuracy by calculating the jump length probability density function as outlined in Ref. 6. Samples with inconsistent jump length patterns were discarded. The mass transport rate, q_s, was calculated from M/BT_o, in which M = total mass collected, B = container width; and T_o = sample collection time. After sieving the collected sand to obtain its grain size distribution, the mass components, M_{ij}, with container number, i, and grain size, j, were also calculated and checked for consistency.

Test Results

The data taken over a 2-yr period are presented in Table 1, where the transport rate calculated from each individual sample is presented, along with the corre-

TABLE 1.—Experimental Data

Sample number (1)	h, in centimeters (2)	V, in centimeters per second (3)	V_*, in centimeters per second (4)	z_o, in millimeters (5)	T, in degrees Celsius (6)	$S_m \times 10^4$ (7)	d_{50}, in millimeters (8)	q_s, in grams per meter-second (9)
2	41	35	3.6	2.8	17	—	0.44	0.63
3	50	34	2.9	1.6	19	—	0.48	0.84
4	58	40	3.0	1.0	20	—	0.44	0.61
6	56	38	3.6	2.4	20	—	0.44	2.07
7	79	39	3.6	4.1	23	—	0.36	2.05
13	99	40	4.4	9.3	19	—	0.40	1.72
14	120	43	5.1	11.0	21	—	0.33	1.12
15	122	46	4.2	4.6	21	—	0.41	7.34
16	65	39	4.2	5.7	22	1.2	0.37	1.01
17	87	39	2.9	5.6	15	1.4	0.33	0.53
19	100	39	3.4	4.5	16.4	1.7	0.30	0.33
20	119	43	4.9	16.2	17.6	1.3	0.31	6.31
22	76	37	2.6	1.1	20.8	1.0	0.30	0.37
23	70	37	3.2	2.4	21	1.0	0.33	1.20
25	67	31	2.9	4.1	21.4	0.8	0.32	0.12
26	56	28	2.2	1.4	21.4	0.8	0.34	0.12
27	79	21	1.9	3.6	21.4	0.5	0.28	0.012
28	46	16	1.7	5.3	22	1.0	0.30	0.0011
29	48	24	2.5	2.3	21.5	1.0	0.32	0.0032
30	59	26	2.4	3.3	21.8	1.0	0.49	0.044
31	60	26	2.4	2.1	21.5	1.0	0.32	0.030
32	75	22	2.4	5.7	21.8	1.0	0.23	0.0059
33	34	19	1.7	1.8	21.8	1.0	0.36	0.0054
34	48	24	1.6	0.3	21.8	1.0	0.32	0.0013
35	60	23	2.3	4.0	21.8	1.0	0.28	0.0030
36	64	23	2.2	2.3	21.8	1.0	0.28	0.0062
37	68	27	1.9	0.3	21.8	1.0	0.36	0.031
39	47	24	2.8	11.7	23.8	0.9	0.34	0.0026
40	57	25	2.5	3.0	23.8	0.9	0.35	0.017
41	59	25	2.6	4.1	23.8	0.9	0.30	0.010
42	74	23	3.1	13.9	23.8	0.9	0.28	0.0052
44	44	25	2.1	1.4	23.8	0.9	0.31	0.0008
45	57	22	1.8	2.7	23.8	0.9	0.36	0.0027
46	63	23	1.6	1.1	23.8	0.9	0.31	0.0029
47	67	27	2.6	6.0	23.8	0.9	0.32	0.040
48	55	19	2.2	9.3	19.4	1.1	0.25	0.0009
49	59	32	2.7	1.8	19.4	1.1	0.31	0.012
51	75	32	3.2	10.3	19.4	1.1	0.31	0.027
52	83	36	3.6	5.1	19.4	1.1	0.33	0.71
54	61	32	3.9	6.0	19.4	1.1	0.32	0.030
55	71	28	3.1	6.0	19.4	1.1	0.33	0.034
56	84	32	2.6	2.2	19.4	1.1	0.30	0.12
57	84	34	3.2	2.1	19.4	1.1	0.33	0.29
58	41	19	1.5	0.3	23.2	1.1	0.31	0.0007

TABLE 1.—*Continued*

(1)	(2)	(3)	(4)	(5)	(6)	(7)	(8)	(9)
60	62	26	2.0	0.4	23.2	1.1	0.34	0.011
61	63	28	2.1	0.6	23.2	1.1	0.32	0.031
62	69	29	3.2	5.5	23.2	1.1	0.32	0.089
64	45	25	2.5	4.6	23.2	1.1	0.32	0.010
65	56	27	2.3	2.1	23.2	1.1	0.35	0.0089
67	69	27	2.4	2.0	23.2	1.1	0.30	0.0039
68	40	20	2.1	3.6	17.6	1.3	0.29	0.0020
69	31	23	2.3	2.6	17.6	1.3	0.29	0.017
70	45	24	2.8	5.0	17.6	1.3	0.30	0.011
71	73	30	3.0	6.8	17.6	1.3	0.30	0.056
73	39	22	1.9	1.8	16	1.1	0.32	0.0019
74	56	20	2.0	3.9	16	1.1	0.28	0.0008
75	55	21	1.7	1.3	16	1.1	0.27	0.0024
76	64	22	2.4	7.3	17	1.1	0.27	0.014
78	37	18	1.7	1.1	17	1.1	0.32	0.0006
79	47	26	3.1	7.0	17	1.1	0.31	0.018
80	49	23	2.9	4.8	17	1.1	0.31	0.031
81	61	22	2.6	8.4	16	1.1	0.23	0.0008

sponding velocity profile parameters and other auxiliary data. Only the measured sediment transport rate is given in the table, although the fractional contributions of the 10 grain sizes in the 30 trap compartments were recorded.

Three different reasons led to the conclusion that the sediment transport data represented primarily bed load. First, visual observation of the sand moving along the bottom showed no sign of suspension since the water was clear. Second, the spacial distribution of the sand in the trap indicated that the jump length of only a small fraction (~0.2%) of the sample was greater than 1,000 particle diameters. Finally, the ratio of the friction velocity to the fall velocity, V_*/w_{50}, was compared to Bagnold's suspension threshold (2), $V_*/w = 1$, and was generally found to be less than that threshold. Nine samples failed to meet the latter two criteria and were omitted from the data set. The resulting transport rate data are therefore considered to be bed-load.

The quality of the data set was studied further by examining the power law relationship between the measured transport rate and the three hydraulic parameters, flow rate per unit width, stream power, and mean velocity. The resulting power laws (in SI units) were

$$q_s = 0.0594 q^{4.27} \quad \ldots \quad (2)$$

$$q_s = 0.00394 (\tau_o V)^{2.79} \quad \ldots \quad (3)$$

and

$$q_s = 5.25 V^{9.36} \quad \ldots \quad (4)$$

The high exponents of these power laws greatly amplify the effects of errors in the hydraulic parameters q, $\tau_o V$, and V. Since the sediment samples were not much larger than the mass in a ripple and the von Karmen constant calculation indicated a velocity error level of 10%, smoothing was used to provide larger samples and more accurate velocities for the evaluation of the predictive

equations. The smoothing was done by ordering the 81 trap samples in accordance with their sediment transport rates, and by averaging each set of five neighboring values of these ordered sediment transport rates and the corresponding hydraulic parameters. The best of the three smoothed relationships, that of the mean velocity, is shown in Fig. 2. The averaging improved the correlation coefficient of this power law from 0.92–0.98.

The comparison between the present data and previous bed-load measurements is best done in a dimensionless format. The bed-load function, ϕ, and the shear

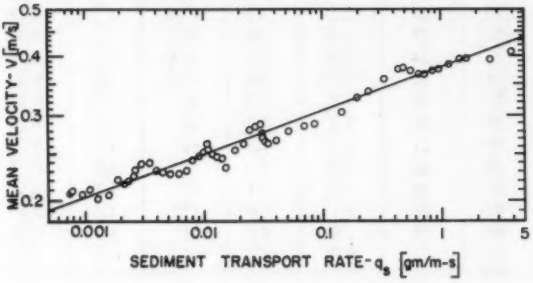

FIG. 2.—Measured Transport Rate

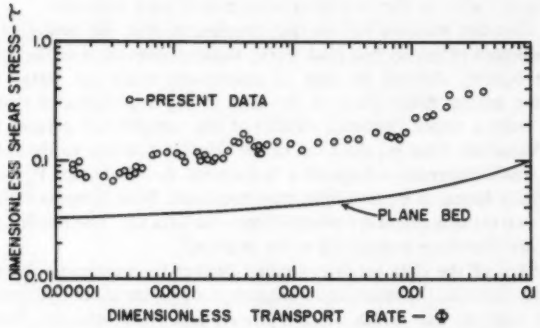

FIG. 3.—Comparison with Previous Data from Vanoni (9)

stress function, τ, are the principal dimensionless variables used in describing bed load

$$\phi = \frac{q_s}{\gamma_s}\left[\left(\frac{\gamma_s}{\gamma} - 1\right) g\, d_{50}^3\right]^{-1/2} \quad \ldots\ldots\ldots\ldots\ldots\ldots\ldots\ldots\ldots\ldots (5)$$

and $$\tau = \tau_o\left[(\gamma_s - \gamma)\, d_{50}\right]^{-1} \quad \ldots\ldots\ldots\ldots\ldots\ldots\ldots\ldots\ldots\ldots (6)$$

In Fig. 3 the smoothed data are compared to previous bed-load data, described

in Ref. 9, for the movement of coarser material over plane beds. The difference between the two data sets is basically due to a Reynolds number effect. The lower Reynolds number ($R = V_* d_{50}/\nu$) of the moving sand was shown by Liu (3) to permit the formation of dunes and ripples, whereas the beds of the earlier tests were planar. The shear stress applied to the sand particles is reduced by the pressure drag of these wave forms. Thus, this Reynolds number effect requires the separation of the bed's drag force into shear drag and form drag and causes the increased scatter seen in the sand transport data in Fig. 3.

Predictions and Observations

The comparison between the sediment movement predicted by the bed-load equations and the observed movement will be presented as a ratio, that is, the predicted transport rate will be divided by the observed transport rate. Since additional details about these equations are available in the works of the original authors and in Ref. 1, only a brief outline of the prediction procedures will be given herein.

The Meyer-Peter and Müller formula (5) for a wide rectangular channel is

$$\gamma \frac{Q_B}{Q}\left(\frac{K_B}{K_G}\right)^{3/2} HS = 0.047\gamma''_s D_E + 0.025\left(\frac{\gamma}{g}\right)^{1/3}(G''_1)^{2/3} \quad \ldots\ldots\ldots (7)$$

in which γ = the specific weight of water; Q_B = the part of the discharge apportioned to the bed and considered responsible for the bed load; Q = the total discharge; K_B = the total roughness coefficient for the bed; K_G = the flat-bed grain roughness; H = the water depth; S = the slope of the energy grade line; γ_s = the specific weight of the sediment; $\gamma''_s = \gamma_s - \gamma$; D_E = the effective diameter of the bed material; g = the acceleration due to gravity; and G''_1 = the bed load weighed under water.

The Meyer-Peter and Müller equation is of the threshold type. The bed load is proportional to the difference between the mean shear stress acting on the grain and the threshold shear stress, raised to the 1.5 power. This threshold stress corresponds roughly to Shield's critical tractive stress. In the application of this equation in the region near the threshold, the transport may appear to be negative. In such cases, the authors of the equation suggested replacing the coefficient 0.047 with 0.030 in Eq. 7, and that procedure was followed herein.

The Meyer-Peter and Müller equation was based on data from experiments with steady, uniform flow in flumes. The range of sediment properties of these tests was such that there was little or no suspended load. The effective diameter of the sediment particles varied between 0.4 mm and 30 mm. This range led to flows both with and without bed waves and so the bedform correction ratio, K_B/K_G, shown in the formula varied between 0.5 and 1.0. This wide range of sediment diameters also covered the cases of both fully-rough bed flow and flow with a viscous sublayer. In the latter case, the authors of the equation recommended the use of the channel Reynolds number and the relative roughness of the bed material to find the friction factor, f, from the Nikuradse diagram. When the roughness, K_G, based on this f was combined in the ratio, K_B/K_G,

this procedure was considered valid for the wide range of sediment movements studied.

The extensive variation of the data base of the Meyer-Peter and Müller equation permits the application of that equation to the sediment movement in Fish Creek. The equation was used to predict the sediment movement based on the smoothed hydraulic data for the creek's flow. These predictions are compared with the measured sediment transport in Fig. 4. The geometric mean value of the ratio of predicted transport to that observed was 1.92, showing the average tendency of the formula to predict excess transport. The ratio's logarithmic standard deviation of 0.29 shows that the scatter in the agreement is a factor of 2.0.

The Toffaleti method for the calculation of bed load (8) is a modification of the Einstein procedure for the calculation of both bed load and suspended load (3). It focuses on channels with sand bottoms, and assumes that part of the sand is moving as bed load and part in suspension. Thus the bed load, BL, is found by evaluating the mass flux, UC, at $y = 2D$, and assuming that

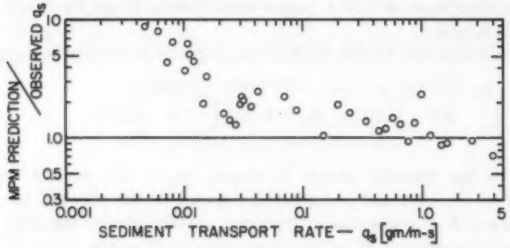

FIG. 4.—Comparison of Meyer-Peter and Müller Prediction with Observed Transport Rate

this flux is constant in the region, $0 \le y \le 2D$, near the bed

$$\mathrm{BL} = C_v \bar{U}\left(\frac{2D}{R}\right)^{Zv} C_L\left(\frac{R}{2D}\right)^{ZL} 2D \quad \ldots\ldots\ldots\ldots\ldots\ldots\ldots\ldots (8)$$

in which $C_v \bar{U}(Y/R)^{Zv}$ = a power law approximation of the velocity profile; and $C_L(R/Y)^{ZL}$ = the sediment concentration distribution. This velocity profile is roughly a 1/7 power law description based on the turbulent boundary layer profile and adjusted for water temperature. The concentration of particles of grain size, D, is determined by equating the suspended load in the region, $2D < y < R/11.24$, with a sediment load, GF, based on Einstein's bed-load function. The variable GF is calculated from

$$GF = 0.60\left(\frac{0.00058\bar{U}^2}{D\,T\,A}\right)^{5/3} \quad \ldots\ldots\ldots\ldots\ldots\ldots\ldots\ldots\ldots\ldots (9)$$

in which T = a function of the water temperature, and A = a measure of the grain shear stress. The ratio, $D\,T\,A/\bar{U}^2$, is based on Toffaleti's unification of Einstein's Y, ξ, and θ into the parameter, A, in order to more simply relate

the grain shear stress parameter, ψ_*, to the overall shear stress variable, ψ.

The three principal differences between Toffaleti's procedure and the Einstein method were: (1) The change of the equation for the velocity distribution from the logarithmic velocity profile to the power law profile; (2) the use of A instead of Y, ξ, and θ; and (3) the use of the suspended load in the region $2D < y < R/11.24$ in evaluating the bed load. The changes were made in order to simplify the original procedure and to optimize the agreement with the more extensive data base used by Toffaleti (8). That base was composed of 239 points from six rivers and 282 points from five flume studies. Like the data base of the Meyer-Peter and Müller formula, this data base provided a broad range of hydraulic variables and sediment transport rates.

The Toffaleti method was applied to the smoothed Fish Creek data, and the resulting ratio of the predicted to observed bed load is shown in Fig. 5. The geometric mean value of that ratio was 1.15, showing close agreement between the Toffaleti predictions and the measured values. The ratio's logarithmic

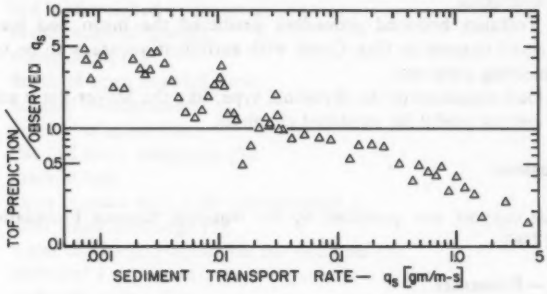

FIG. 5.—Comparison of Toffaleti Prediction with Observed Transport Rate

standard deviation of 0.39 shows a scatter in this agreement of a factor of 2.5.

Analysis and Conclusions

The goal of this paper, the evaluation of bed-load equations, requires accurate data for both the channel's hydraulic parameters and the sediment transport rate. The experimental procedure presented here met that need by measuring the flow and sediment transport in detail, by using a variety of internal accuracy checks, and by averaging the data to reduce its scatter. The best evidence of the quality of the resulting data is the correlation coefficient of 0.98 between the bed load and the mean velocity.

The comparisons between predicted and measured bed loads show that the Toffaleti method is the better predictor of the bed load of sand-bottomed channels. However, it is obvious from Fig. 5 that the scatter in the agreement between the predicted and observed values of q_s is much higher than the scatter of the basic data, as shown in Fig. 2. Since both the Toffaleti method and the best power law description of the current data are based principally on the

mean velocity, the additional scatter could be associated with the effects of the grain size, water depth, and temperature, and the slope of the local energy grade line used in the Toffaleti procedure, or with the randomness of the bed load. The Meyer-Peter and Müller predictions were significantly higher than the measured sediment transport rates. Further, their method predicted zero movement in many cases where movement was observed. This effect of the threshold type of predictive equation is especially troublesome when bed forms are present, since the separation of form drag from bed particle drag makes the location of the threshold more difficult. These problems demonstrate that the Meyer-Peter and Müller equation should not be used for sand bottomed channels.

The conclusions of this evaluation are:

1. The measurement procedure, using the velocity profiles and the compartmented sediment trap, provides the accuracy and the self-consistency needed for reliable bed-load measurement, provided that sufficient samples are taken to permit averaging.
2. The Toffaleti bed-load procedure predicted the mean bed load in the sand-bottomed channel at Fish Creek with sufficient accuracy to be useful for most engineering purposes.
3. Bed-load equations of the threshold type, like the Meyer-Peter and Müller equation, are not useful for sand-bed channels.

Acknowledgment

Financial support was provided by the National Science Foundation Grant ENG 76-17263.

Appendix I.—References

1. Amin, M. I., "The Compartmented Bed-Load Trap and its Use in Comparing the Bed-Load Formulae," thesis presented to Cornell University, at Ithaca, N.Y., in 1980, in partial fulfillment of the requirements for the degree of Doctor of Philosophy.
2. Bagnold, R. A., "The Nature of Saltation and of 'Bed-Load' Transport in Water," *Proceedings of the Royal Society*, London, England, Series A, Vol. 332, 1973, pp. 473–504.
3. Einstein, H. A., "The Bed Load Function for Sediment Transportation in Open Channel Flows," *Soil Conservation Service Bulletin No. 1026*, United States Dept. of Agriculture, Washington, D.C., Sept., 1950.
4. Liu, H. K., "Mechanics of Sediment-Ripple Formation," *Journal of the Hydraulics Division*, ASCE, Vol. 83, No. HY2, Proc. Paper 1197, Apr., 1957, pp. 1194-1–1197-23.
5. Meyer-Peter, E., and Müller, R., "Formulas for Bed Load Transport," *Proceedings*, Second Meeting of the International Association for Hydraulic Structures Research, June, 1948, pp. 39–64.
6. Murphy, P. J., and Amin, M. I., "Compartmented Sediment Trap," *Journal of the Hydraulics Division*, ASCE, Vol. 105, No. HY5, Proc. Paper 14577, May, 1979, pp. 489–500.
7. Shen, H. W., ed., *River Mechanics*, Water Resources Publications, Fort Collins, Colo., 1971.
8. Toffaleti, F. B., "Definitive Computations of Sand Discharge in Rivers," *Journal of the Hydraulics Division*, ASCE, Vol. 95, No. HY1, Proc. Paper 6350, Jan., 1969, pp. 225–248.
9. Vanoni, V. A., ed., *Sedimentation Engineering*, Manual No. 54, ASCE, New York, N.Y., 1975.

APPENDIX II.—NOTATION

The following symbols are used in this paper:

A = bed roughness parameter (8);
B = width of compartment of trap;
BL = bed load (8);
C = sediment concentration (8);
C_V = velocity coefficient (8);
C_L = sediment concentration coefficient (8);
D = grain size (8);
D_E = effective diameter of bed material (5);
d = grain sieve diameter;
$F4$ = constant of integration (8);
f = friction factor;
GF = sediment load based on Einstein's ϕ (8);
G_1'' = bed load weighed under water (5);
g = acceleration of gravity;
H = water depth (5);
h = depth of open channel flow;
i = number of container;
j = number of grain size;
K_G = flat-bed grain roughness (5);
M = mass in trap;
M_{ij} = mass of grain size, j, in compartment, i;
Q = total water discharge (5);
Q_B = water discharge responsible for bed load (5);
q_s = sediment's mass transport rate per unit width;
R = hydraulic radius (8);
R = particle Reynolds number;
S = slope of energy grade line (5);
S_m = mean slope of channel;
T = water temperature;
T_o = duration of interval when trap is open;
U = local velocity (8);
$\bar{U}$ = mean velocity (8);
$U(z)$ = velocity of fluid at height, z, above bed;
V = mean velocity of fluid;
V_* = friction velocity;
w = fall velocity;
w_{50} = fall velocity of d_{50} particle;
Y = elevation above bed (8);
YA = elevation at point YA (8);
ZV = exponent of velocity distribution (8);
ZL = exponent of concentration distribution (8);
z_o = roughness length of velocity profile;
γ, γ_s = specific weight of sediment and water;
κ = von Karmen's constant;
ν = kinematic viscosity;

ρ = density of fluid;
τ = dimensionless shear stress;
τ_o = bed shear stress; and
ϕ = dimensionless sediment transport rate.

VERTICAL VELOCITY PROFILES IN STRATIFIED FLOWS

By Steve C. McCutcheon,[1] A. M. ASCE

INTRODUCTION

Flows stratified by heat, dissolved solids, and suspended solids are quite common in the natural environment. These include flows in the atmospheric boundary layer, rivers, lakes, estuaries, and oceans. The vertical transport of the stratifying agent and momentum depend on the shape of the vertical velocity profile.

The study described by this paper focuses on the shape of the vertical velocity profile in a unidirectional, 2-dimensional, turbulent, fully developed, continuously stratified flow. For this case, the turbulence in the flow is generated by the movement of fluid over a rough boundary. The dimensional analysis of Monin and Obukhov (10) is employed to extend the Prandtl-von Karman velocity law to stratified flows. The buoyancy flux is related to the velocity and density gradient such that the original Monin-Obukhov similarity analysis is extended to flows in which the buoyancy flux may vary over the depth. Emphasis is placed on open-channel flows; therefore, flows in a laboratory flume stratified by salt are used for verification.

PREVIOUS WORK

Several studies have considered turbulent stratified flows over a rough boundary, but the results of these studies are conflicting. To define and resolve this conflict, it is useful to introduce a schematic definition of expected vertical velocity profiles in stratified flows, shown in Fig. 1. Stable stratification describes a flow in which lighter layers of fluid move over heavier layers and vice versa for unstable stratification. Neutral stratification implies a well mixed or homogeneous flow.

Fig. 1 follows from extensive studies in the 2-dimensional, stratified, atmospheric boundary layer (18). Schiller and Sayre (14), Hwang (6), the writer (8), Odd and Rodger (12), Vanoni (20), and Einstein and Chien (3) have measured

[1]Hydrologist, U.S. Geological Survey, Gulf Coast Hydroscience Center, NSTL Station, Miss.

Note.—Discussion open until January 1, 1982. To extend the closing data one month, a written request must be filed with the Manager of Technical and Professional Publications, ASCE. Manuscript was submitted for review for possible publication on April 8, 1980. This paper is part of the Journal of the Hydraulics Division, Proceedings of the American Society of Civil Engineers, ©ASCE, Vol. 107, No. HY8, August, 1981. ISSN 0044-796X/81/0008-0973/$01.00.

velocity profiles in stably stratified wide open-channel flows that resemble curve type 2 in Fig. 1. Odd and Rodger measured vertical velocity profiles in a wide estuary during ebb tide. Schiller and Sayre and Hwang studied heat stratified flows in a flume; the writer studied a salt stratified flow in a flume; and Vanoni and Einstein and Chien studied suspended-sediment stratified flows in flumes.

Flume studies by French (4) and Majewski (9,10) in narrow flumes do not agree with the studies previously mentioned. French studied stable salt-stratified flows and Majewski studied stable heat-stratified flows. French and Majewski measured velocity profiles in stable stratified flows that have the general shape of curve 3 rather than curve 2.

This conflict can be resolved by considering the width-to-depth ratios and the level of stratification. From the summary of the various studies of stratified flows given in Table 1, it is evident that nonrepresentative velocity profile shapes occur in open channels with width-to-depth ratios of 4.3 and less. Studies by Majewski are enlightening. Majewski ran control experiments with unstratified flows that document sidewall influence and strong secondary currents in his narrow channels. It is hypothesized that the nonrepresentative velocity profiles

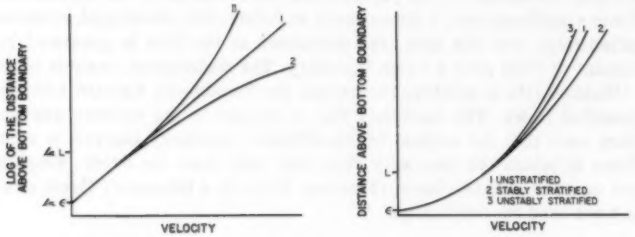

FIG. 1.—Three Types of Velocity Profiles Expected in 2-Dimensional Stratified Flows

in narrow stratified flows are a result of the three-dimensional effects similar to those recorded in Majewski's control experiments.

The work by Schiller and Sayre also indicates that the level of stratification may also lead to nonrepresentative velocity profiles in wider channels, as shown in Fig. 2. Fig. 2 shows the shape of vertical velocity and temperature profiles along the channel center line from the work of Schiller and Sayre. When a high temperature difference exists over the depth, the velocity profile shapes follow those of French and Majewski. Discounting entrance effects, it is hypothesized that stratification magnifies sidewall influence.

The results of Kantha et al. (7) better illustrate the influence of geometry in stratified flows. Kantha et al. studied a stratified flow in an annular tank. Turbulence was input through the water surface by a grid moving over the surface. The growth of a well-mixed layer below the surface was related to the shearing rate. Fig. 3 shows the results of Kantha et al. There are no geometry effects at a gross Richardson number of 36. At higher Richardson numbers, sidewall effects in the annular tank become significant. Therefore, geometry and the level of stratification are important in producing 2-dimensional, turbulent, stratified flows.

A number of expressions have been put forth to describe vertical profiles in stratified flows. The Monin-Obukhov similarity analysis (11) results in a velocity profile expression that has been verified by Webb (21) and others (11) for the atmospheric boundary layer in which the buoyancy flux is essentially constant with distance above the bottom boundary. Hwang (6) applied the Monin-Obukhov analysis to open-channel flows with very limited results. Hwang assumed a constant buoyancy flux and theorized that the momentum transfer is unaffected by stratification. Schiller and Sayre (14) derived a profile expression from the Reynolds equations that is based on the Boussinesq approximation (small density changes have no inertia effects), and this expression predicts a decrease in

TABLE 1.—Summary of Studies in Stably Stratified Flows

Investigator (1)	Width-to-depth ratio (2)	Stratifying agent (3)	Experimental device (4)	Curve type (5)
French (4)	1.8–0.8	salt	flume	3
Majewski (9)	3.6–4.3[a]	heat	hydraulic model	3
Majewski (10)	1.24, 2.07, 3.10	heat	flume	3
Hino, et al. (5)	1.1, 2.4, 3.3	salt and sugar	flume	—[b]
Schiller and Sayre (14)	5.0, 10.0	heat	flume	2
Hwang (6)	5.0	heat	flume	2
Monin and Yaglom (11)	∞	heat	atmospheric boundary layer	2
Webb (21)	∞	heat	atmospheric boundary layer	2
Chuang and Cermak (2)	3.0[c]	heat	wind tunnel	2
SethuRaman and Cermak (15)	9.0–16.0[c]	heat	wind tunnel	2
Plate and Lin (13)	63.2–5.7[c]	heat	wind tunnel	2
Odd and Roger (12)	20–100	salt	estuary	2
Vanoni (19)	11.8–5.0	suspended sediment	flume	2
McCutcheon (8)	4.4, 8.0	salt	flume	2

[a] Based on the average width of the trapezoid sections.
[b] Inconclusive information.
[c] Based on the boundary layer thickness.

velocities near the boundary due to stable stratification. This prediction is not borne out by experimental evidence.

French (4) also applied the Monin-Obukhov analysis to develop a velocity profile for stratified flows, but unlike Hwang (6) he avoided the assumptions of a constant buoyancy flux and unaffected momentum transfer by stratification. The development in the following paragraphs follows French's development in many details, but French empirically modified the definition of the Monin-Obukhov scaling length for stratified flows to match his nonrepresentative narrow

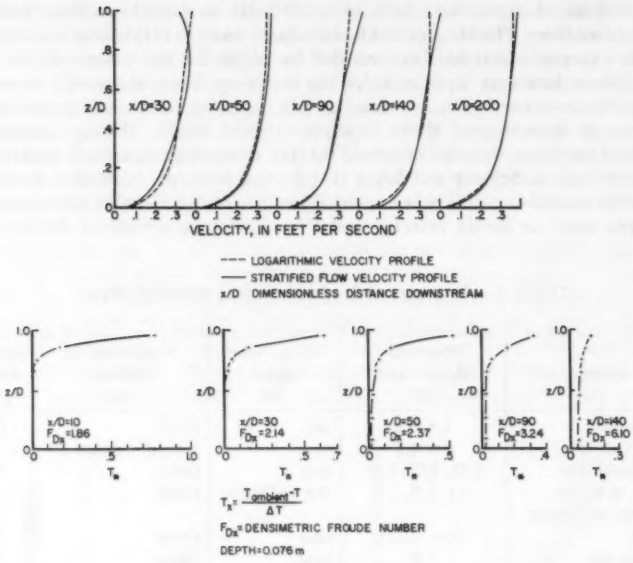

FIG. 2.—Velocity and Temperature Profiles Measured by Schiller and Sayre (14) at Flume Center Line

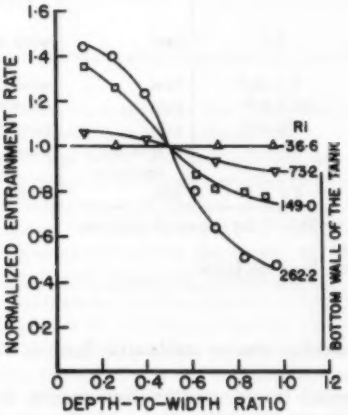

FIG. 3.—Entrainment Rate as Function of Depth-to-Width Ratio for Various Gross Richardson Numbers, $R_i = Dg\Delta\rho/\bar{\rho}\,u_*^2$, for Stratification by NaCl. Entrainment Rate Normalized by Values at Depth/Width = 0.5 and $u_*^2 = 1.41$ cm/s. Adapted from Kantha et al. (7)

flume velocity profiles. Therefore, the following analytical development strives to rectify problems encountered by French and Hwang.

Analytical Development

The vertical velocity profile in unstratified flows has been the focus of several studies (19,13), from which it can be concluded that the velocity profile in hydraulically rough, 2-dimensional, unstratified flows can be described by the Prandtl-von Karman velocity law

$$u(z) = \frac{u_*}{k} \ln \frac{z}{\epsilon} \quad \ldots \ldots \ldots

and the velocity profile can be described by Eq. 1. Since this dimensional analysis has focused on the shape of the velocity profile, $\partial u/\partial z$, it can be hypothesized that a dimensionless combination of $\partial u/\partial z$, u_*, and z is related to some function of ζ

$$\frac{\partial u}{\partial z}\frac{zk}{u_*} = \Phi(\zeta) \quad \ldots \ldots \ldots

$$\frac{\partial u}{\partial z} = \frac{u_*}{kz}\left(\frac{1}{1 + \dfrac{\alpha g k^2 z^2}{\bar{\rho} u_*^2}\dfrac{\partial \rho}{\partial z}}\right) \quad \ldots\ldots\ldots\ldots\ldots\ldots\ldots\ldots\ldots\ldots \quad (11)$$

in which $\alpha = c\alpha_1$. Thus the shape of the velocity profile is related to the shape of the density profile. Furthermore, for unstratified flow, in which $\partial\rho/\partial z = 0$, Eq. 11 reduces to the Prandtl-von Karman velocity law, Eq. 6.

Eq. 11 can be solved for a velocity profile expression when the shape of the density profile is defined. Since many open-channel density profiles are nonlinear, it is useful to consider a general case in which $\partial\rho/\partial z = f(z)$, resulting in

$$\frac{u(z_l)}{u_*} = \frac{1}{k}\int_{\epsilon}^{z_l} \frac{dz}{z\left[1 + \dfrac{\alpha g}{\bar{\rho} u_*^2} k^2 z^2 f(z)\right]} \quad \ldots\ldots\ldots\ldots\ldots\ldots\ldots\ldots \quad (12)$$

in which $f(z)$ is negative for a stable density gradient, forcing the denominator to be less than one. Therefore, the right side of Eq. 12 is greater than

$$\frac{1}{k}\int_{\epsilon}^{z_l} \frac{dz}{z} = \frac{1}{k}\ln\frac{z}{\epsilon} \quad \ldots\ldots\ldots\ldots\ldots\ldots\ldots\ldots\ldots\ldots\ldots\ldots \quad (13)$$

indicating that a stable density gradient leads to an increase in velocity over what would be expected if density stratification did not exist. Therefore, Eq. 12 follows the expectations for stratified flows first expressed by Taylor (16). Taylor found that stable stratification inhibits momentum transfer.

If the density profile can be approximated as a straight line, $\partial\rho/\partial z = \beta$, the velocity profile can be expressed as

$$\frac{u(z)}{u_*} = \frac{1}{k}\ln\left[\frac{\left(\dfrac{z}{\epsilon}\right)^2 + \dfrac{g\alpha\beta}{\bar{\rho} u_*^2} k^2 z^2}{1 + \dfrac{g\alpha\beta}{\bar{\rho} u_*^2} k^2 z^2}\right]^{1/2} \quad \ldots\ldots\ldots\ldots\ldots\ldots\ldots \quad (14)$$

It is important to note that the denominator in Eq. 12 differs by sign with the similar velocity profile expression of French (4) because French incorrectly defined the Monin-Obukhov scaling length. The coefficient α is also different by the factor c. French's velocity profile expression indicates that stable stratification increases momentum transport. This must be attributed to sidewall influence.

Having improved upon the approach of Hwang and corrected a sign difference introduced by French, it is necessary to verify Eqs. 12 and 14 with two-dimensional, stratified, open-channel data. The next section describes data collected by the writer for that purpose.

Laboratory Experiments

To verify Eqs. 12 and 14, a series of laboratory experiments was carried out in a flume 0.6 m wide, 0.3 m deep, and 18.3 m long. Saline water was

injected underneath fresh water simultaneously with the use of a splitter plate to produce stably stratified flows, as shown in Fig. 4. The flume was operated

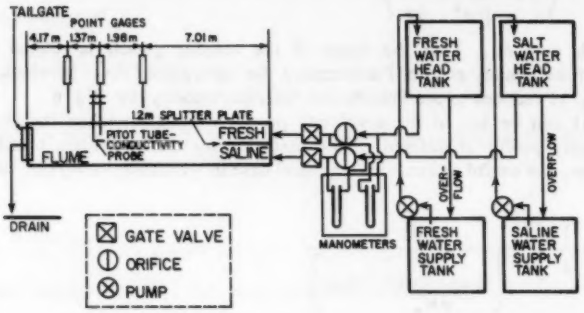

FIG. 4.—Experimental Equipment Utilized for Stratified Flow Experiments

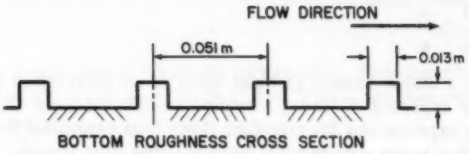

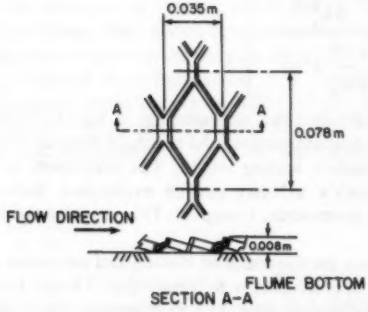

FIG. 5.—Bottom Roughness Used in Flume Studies

in a once-through mode with experimental times of 9 min and 17 min. These times were determined by discharge and saline water storage capacity. Experiments varied depth of flow, discharge, bottom roughness patterns, and density

difference over the depth. Depths were approximately 0.08 m and 0.14 m with corresponding discharges of 0.144 m^3/sec and 0.0074 m^3/sec. Bottom roughness was of two types. One consisted of an expanded metal mesh or plaster lath and the other consisted of 0.013-m wooden strips on 0.051-m centers, as shown in Fig. 5. Density profile shapes were controlled by varying the initial density difference and by controlling the interfacial mixing at the end of the splitter plate. Salinity was the sole stratifying agent; heat stratification was avoided. Density profiles varied from two-layer profiles to linear density profiles. Values of z/L varied from 0–4.5.

Point velocities were measured over the depth at the flume center line with a Prandtl type 1/8 in. (3.2 mm) diameter pitot-static tube connected by an airless water column to a P90D Celesco variable reluctance, ±1 in. (25.4 mm) range, differential pressure transducer. (The use of the brand name in this report is for identification purposes only and does not imply endorsement by the U.S. Geological Survey.) Densities were deduced from saline solution electrical conductivity measured at the same time with a custom made probe described by Anderson et al. (1). The probe consisted of a hypodermic syringe as one pole with an insulated platinum wire in the center extending out of the needle to make up a second pole. The change in voltage across these two poles was related to solution conductivity through an extensive calibration. These profiles were simultaneously measured 7.0 m downstream of the splitter plate.

Water surface slopes were computed from water-surface elevations measured with standard point gages [0.001 ft (0.000305 M) graduations] over a 3.35-m reach approximately centered about the point where velocity and density profiles are measured. The gages were mounted over the flume center line. Discharge was measured with orifice meters in the fresh-water and saline-water supply lines.

Several observations give assurance that experiments were properly designed to verify Eqs. 12 and 14. Each experimental combination of depth, discharge, and bottom roughness was applied first to an unstratified flow and then to stratified flows. These unstratified control experiments, along with boundary layer calculations, indicated that the bottom boundary layer was fully developed for unstratified flows. Then velocity profiles, measured across the flume at the test section, showed negligible influence from secondary circulation in unstratified control experiments. Finally, a fluorescent dye added to the saline-water supply quickly became completely mixed over the depth in unstratified control experiments. For stratified flows, the dye penetrated to the water surface but remained stratified. Eddies generated at the bottom were visually observed to penetrate the less dense upper layer until eddies reached the water surface. The fluorescent dye and the density difference between the eddy and surrounding waters made it possible to track large eddies.

The density difference between the upper layer and lower layer was decreased until eddies could be observed moving from the bottom to the water surface at a point well upstream of the test section. This practice gave some assurance that velocity profiles were controlled by bottom-generated turbulence. The concept of uniform flow cannot be applied to stratified flows in which the density profile decays in the downstream direction. However, in areas where bottom generated turbulence migrates over the depth flow causing density changes at all depths, Eqs. 12 and 14 should be valid.

TABLE 2.—Hy

Experiment number (1)	Discharge, in cubic meters per second (2)	Depth, in meters (3)	Slope $\times 10^{-3}$ (4)	Temperature, in degrees Celsius (5)	Roughness scale, in meters (6)
					(*a*) Wooden Strip
RUN 2/13/3	0.0144	0.092	2.436	5.0	0.00386
RUN 2/22/1	0.0144	0.089	2.455	7.0	0.00530
RUN 2/13/2	0.0144	0.090	2.209	5.0	0.00404
RUN 2/16/1	0.0074	0.077	1.291	6.4	0.00463
RUN 2/15/1	0.0074	0.077	1.109	6.0	0.00397
RUN 2/15/2	0.0074	0.076	0.973	5.5	0.00519
RUN 2/20/3	0.0144	0.145	0.391	5.1	0.00336
RUN 2/20/2	0.0144	0.145	0.391	5.7	0.00398
RUN 2/21/2	0.0074	0.141	0.127	6.0	0.00432
RUN 2/21/1	0.0074	0.140	0.082	7.4	0.00653
RUN 2/20/4	0.0074	0.139	0.018	5.3	0.00706
					(*b*) Expanded Metal
RUN 2/7/2	0.0144	0.088	2.564	5.5	0.00487
RUN 2/6/1	0.0144	0.084	2.564	5.3	0.00421
RUN 2/6/2	0.0144	0.082	2.500	5.2	0.00452
RUN 2/5/3	0.0074	0.080	0.855	5.6	0.00537
RUN 2/5/2	0.0074	0.078	0.636	6.4	0.00645
RUN 2/5/1	0.0074	0.077	0.709	7.0	0.00603
RUN 12/19/3	0.0144	0.140	0.327	10.6	0.00496
RUN 1/22/2	0.0144	0.144	0.282	7.0	0.00451
RUN 12/20/1	0.0144	0.143	0.364	11.2	0.00547
RUN 11/10/2	0.0074	0.140	0.118	16.3	0.00479
RUN 12/14/2	0.0074	0.140	0.055	11.0	0.00361

Note: 1 m = 3.28 ft; 1 kg/m^3 = 0.00194 slugs/ft^3.

Results

Data collected for each experiment included velocity profiles and density profiles at the flume center line 7.0 m downstream of the splitter plate, water surface slope over a 3.4 m reach approximately centered about that point, discharge, water temperature, and depth of flow. Table 2 presents these data and the resulting reduced data.

The reduced data include the roughness scale, shear velocity, average velocity and density in the vertical at the flume center line, Reynolds number, and friction factor. The roughness scale and shear velocity were calculated using the two to four lowest points on the measured velocity profile for stratified flows. The roughness scale and shear velocity were also determined from unstratified control experiments for the purpose of comparison. Shear velocities varied slightly with stratification, but control experiments served as rough benchmarks for the rejection of experiments with questionable shear velocity measurements.

draulic Data

Shear velocity, in meters per second (7)	Average velocity, in meters per second (8)	Average density, in kilograms per cubic meter (9)	Reynolds number, $4\ UD/\nu \times 10^4$ (10)	$8(u_*/U)^2$ (11)
Roughness				
0.0549	0.288	999.65	6.97	0.291
0.0667	0.318	1,005.47	7.92	0.351
0.0589	0.329	1,004.02	7.79	0.257
0.0430	0.196	999.90	4.13	0.380
0.0404	0.204	1,002.54	4.25	0.314
0.0400	0.184	1,004.03	3.73	0.382
0.0310	0.210	1,000.04	8.07	0.169
0.0275	0.202	1,002.58	7.86	0.148
0.0170	0.108	999.86	4.12	0.193
0.0153	0.098	1,001.66	3.86	0.222
0.0204	0.113	1,001.06	4.16	0.196
Mesh Roughness				
0.0630	0.303	999.83	7.11	0.342
0.0600	0.308	1,004.91	6.85	0.344
0.0619	0.307	1,004.40	6.67	0.325
0.0390	0.172	999.83	3.69	0.409
0.0416	0.173	1,003.29	3.70	0.405
0.0389	0.173	1,003.74	3.73	0.462
0.0283	0.168	1,001.35	7.29	0.227
0.0271	0.195	1,002.78	7.85	0.154
0.0284	0.165	1,002.78	7.43	0.236
0.0160	0.097	1,000.57	5.00	0.218
0.0155	0.112	1,001.42	4.94	0.154

The roughness scale and shear velocity determinations should not be affected by stratification. This was checked by comparing the velocity predictions of Eq. 1 (unstratified) and Eq. 12 (stratified) at all the points near the bottom used to calculate the roughness scale and shear velocity. The greatest difference between Eqs. 1 and 12 was found to be 4%. This indicates that stratification did not significantly bias the determinations of the roughness scale and shear velocity.

Twenty-two velocity profiles (109 velocity measurements) measured in unstratified and stratified flows are presented in Ref. (8). Fig. 6 represents a typical example. Here a measured velocity profile (circles) is plotted on semilogarithmic and arithmetic scales and compared to the predictions of Eqs. 1, 14, and 12. This example indicates that Eqs. 12 and 14 are better predictors of velocity profiles in stratified flows than Eq. 1.

This is better illustrated by considering pairs of dimensionless velocities (u/u_*) consisting of a measured value and a predicted value. Table 3 gives the mean differences between measured dimensionless velocities and predicted dimension-

less velocities using: (1) Eq. 1; (2) Eq. 14; and (3) Eq. 12. A *t*-test of the means indicated a significant difference in measured velocity and predicted velocity, using Eq. 1, whereas there is not a significant difference in measured velocity and predicted velocity using Eq. 12 or Eq. 14.

Prior to evaluating Eqs. 12 and 14, the Monin-Obukhov power series coefficient, α, was evaluated as 5.8 ± 0.3 from the laboratory data generated in this study.

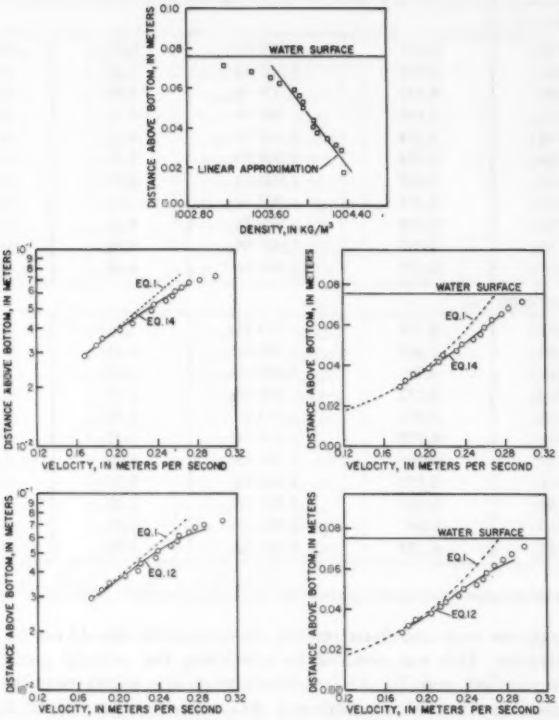

FIG. 6.—Typical Density Profile with Linear Approximation and Comparison of Typical Measured Velocity Profile with Eqs. 1, 14, and 12 on Semilogarithmic and Arithmetic Scales

The value of α, the maximum value of z/L, and the fit of Eqs. 12 and 14 to the measured data are interrelated and inseparable. Eqs. 12 and 14 can fit data with large z/L (>0.0025) by decreasing α, but this violates two assumptions of Eqs. 12 and 14: (1) Eq. 8 is limited to small z/L; and (2) the variable in Eq. 8 is z/L, not α. For these laboratory data, large z/L can be accommodated only if α varies with the maximum z/L. Therefore, the maximum z/L was decreased incrementally to 0.0025 until α did not vary as a function of $(z/L)_{max}$.

α was evaluated by changing that coefficient until the parameter

$$\frac{\sum_{i=1}^{i=n}\left[\left(\frac{u}{u_*}\right)_{\text{meas}}-\left(\frac{u}{u_*}\right)_{\text{pred}}\right]_i}{n} \quad \ldots\ldots\ldots\

Conclusions

The importance of the width-to-depth ratio in stratified flow is noted from previous studies. Stratified flows in narrow flumes are characterized by peculiar vertical velocity profiles if the width-to-depth ratio is 4.3 or less. In addition, 3-dimensional effects occur in wider flows when the stratification is highly stable.

The studies presented here have demonstrated the application of the Monin-Obukhov analysis in predicting velocity gradients and velocity profiles in stably stratified flows with $z/L \leq 0.025$. A t-test for paired data indicates the Prandtl-von Karman velocity law is not applicable to stratified flows, whereas velocity profile expressions, modified with the Monin-Obukhov scaling length, L, do describe velocity gradients and vertical profiles in stably stratified flows. Improved expressions for $\partial u/\partial z$ can lead to a better description of vertical mixing.

The coefficient for a linear approximation of the Monin-Obukhov function has been evaluated as 5.8 ± 0.3, which is comparable to the widely accepted value of 5.2 ± 0.5 for atmospheric boundary layer flows.

Finally, these results demonstrate the importance of z/L in stratified, open-channel flows and indicate that turbulent, 2-dimensional, stratified flows over a rough boundary in an open channel are similar to atmospheric boundary layer flows. Previous work by French (4) in a narrow flume is not valid for 2-dimensional stratified flows. French incorrectly defined the Monin-Obukhov scaling length.

Acknowledgments

This work has been supported by the U.S. Geological Survey thesis support program during the writer's studies at Vanderbilt University in Environmental and Water Resources Engineering. Advice was received from Richard French, advisor, now at the University of Nevada, Frank Parker at Vanderbilt University, and Stanley Sauer, Robert Baker, Verne Schneider, and Harvey Jobson, all of the U.S. Geological Survey. Appreciation is expressed for reviews offered by Edmund Prych, U.S. Geological Survey, Dave McIntosh, Tennessee Valley Authority, and Richard French.

Appendix I.—References

1. Anderson, J. L., Parker, F. L., and Benedict, B. A., "Negative Buoyant Jets in a Cross Flow," *EPA-660/2-73-012*, U.S. Environmental Protection Agency, Washington, D.C., Oct., 1973, pp. 56–61.
2. Chuang, H., and Cermak, J. E., "Similarity of Thermally Stratified Shear Flows in the Laboratory and Atmosphere," *The Physics of Fluids Supplement: Boundary Layers and Turbulence*, Vol. 10, 1967, pp. S255–S258.
3. Einstein, H. A., and Chien, N., "Effects of Heavy Sediment Concentration Near the Bed on the Velocity and Sediment Distribution," *Sediment Series No. 8*, U.S. Army Corps of Engineers, Missouri River Division, Omaha, Neb., 1956.
4. French, R. H., "Stratification and Open Channel Flow," *Journal of the Hydraulics Division*, ASCE, Vol. 104, No. HY1, Proc. Paper 13458, Jan., 1978, pp. 21–32.
5. Hino, M., Shikata, H., and Nakai, M., "Large Eddies in Stratified Flow," *Proceedings of the 12th International Association for Hydraulic Research*, Sept., 1967, pp. 61–73.
6. Hwang, G., "Buoyancy Effects in Thermally Stratified Open-Channel Flow," thesis presented to the University of Iowa, at Iowa City, Iowa, in 1975, in partial fulfillment of the requirements for the degree of Doctor of Philosophy.
7. Kantha, L. H., Phillips, O. M., and Azad, R. S., "On Turbulent Entrainment at

a Stable Density Interface," *Journal of Fluid Mechanics*, Vol. 79, Part 4, Mar., 1977, pp. 753–768.
8. McCutcheon, S. C., "The Modification of Vertical Velocity Profiles by Density Stratification," thesis presented to Vanderbilt University, at Nashville, Tenn., in 1979, in partial fulfillment of the requirements for the degree of Doctor of Philosophy.
9. Majewski, W., "Laboratory Investigation on Heat Transfer in Thermally Stratified Flow," *Proceedings of the 14th Congress of the International Association for Hydraulic Research*, August 29–September 3, 1971, pp. 207–216.
10. Majewski, W., "Modeling of Heated Water Discharges into River," *International Symposium on Stratified Flows, Novosibirsk, USSR, International Association for Hydraulic Research*, Aug. 29–31, 1972, pp. 383–395.
11. Monin, A. S., and Yaglom, A. M., *Statistical Fluid Mechanics: Mechanics of Turbulence*, J. L. Lumley, ed., Vol. 1, The M.I.T. Press, Cambridge, Mass., 1971, pp. 425–486.
12. Odd, N. V., and Rodger, J. G., "Vertical Mixing in Stratified Tidal Flows," *Journal of the Hydraulics Division*, ASCE, Vol. 104, No. HY3, Proc. Paper 13599, Mar., 1978, pp. 337–351.
13. Plate, E. H., and Lin, C. W., "Investigations of the Thermally Stratified Boundary Layer," *Fluid Dynamics and Diffusion Laboratory Paper No. 5*, Colorado State Univ., Fort Collins, Colo., 1966.
14. Schiller, E. J., and Sayre, W. W., "Vertical Mixing of Heated Effluents in Open-Channel Flow," *Iowa Institute of Hydraulics Research Report No. 148*, Univ. of Iowa, Iowa City, Iowa, Sept. 1973.
15. SethuRaman, S., and Cermak, J. E., "Stratified Shear Flows over a Simulated Three-Dimensional Urban Heat Island," *Fluid Dynamics and Diffusion Laboratory Technical Report No. 23*, Univ. of Colorado, Fort Collins, Colo., Aug., 1973, pp. 1–186.
16. Taylor, G. I., "Effect of Variation in Density on the Stability of Superposed Streams of Fluid," *Proceedings of the Royal Society, London Series A*, Vol. 132, 1931, pp. 499–523, reprinted in *G. I. Taylor: Scientific Papers*, G. K. Batchelor, ed., Vol. 2, Cambridge University Press, Cambridge, England, 1960, pp. 219–239.
17. Taylor, R. J., "Similarity Theory in the Relation Between Fluxes and Gradients in the Lower Atmosphere," *Quarterly Journal of the Royal Meteorological Society*, Vol. 86, 1960, pp. 67–78.
18. Turner, J. S., *Buoyancy Effects in Fluids*, Cambridge University Press, Cambridge, England, 1973, pp. 128–134.
19. Vanoni, V. A., "Velocity Distribution in Open-Channels," *Civil Engineering*, Vol. 11, No. 6, June, 1941, pp. 356–357.
20. Vanoni, V. A., "Transportation of Suspended Sediment by Water," *Transactions of the American Society of Civil Engineers*, Vol. 111, 1946, pp. 67–133.
21. Webb, E. K., "Profile Relationships: The Log-Linear Range, and Extension to Strong Stability," *Quarterly Journal of the Royal Meteorological Society*, Vol. 96, 1970, pp. 67–90.

Appendix II.—Notation

The following symbols are used in this paper:

B = buoyancy flux;
c = ratio of mass to momentum mixing lengths;
D = depth of flow;
F_{DX} = densimetric Froude number;
$f(z)$ = function of z describing density gradient;
g = local acceleration of gravity;
k = von Karman's constant (= 0.4);
L = Monin-Obukhov scaling length;
ℓ = momentum mixing length;
ℓ_m = mass mixing length;

n = number of measurements;
R_i = gross Richardson number;
T = temperature of water;
$T_{ambient}$ = ambient temperature;
$T_* = (T_{ambient} - T)/\Delta T$ = dimensionless temperature;
$u(z)$ = velocity in horizontal direction;
u_* = shear velocity;
U = average velocity at flume center line;
w' = fluctuation of vertical velocity;
x = distance downstream;
z = distance above bottom;
α = Monin-Obukhov power series coefficient;
β = constant density gradient;
ΔT = temperature difference over depth;
ϵ = roughness scale;
ζ = dimensionless distance, z/L;
ν = kinematic viscosity;
ρ = density, overbar denotes depth average, prime denotes density fluctuation; and
Φ = function of z/L.

TURBULENCE MODEL FOR FLOW OVER DREDGED CHANNELS

By C. Koutitas,[1] M. ASCE and B. O'Connor[2]

INTRODUCTION

The dredging of channels in alluvial material is a common feature of many marine and river engineering schemes. Particular examples are the lengthening and deepening of port approach channels, due to the increasing size of modern bulk carriers, and the construction of dredged trenches across estuaries and rivers in order to bury pipelines. Unfortunately, many such dredged channels are alined at an angle to the flow of sediment, and this alinement can produce high siltation rates. Often, channels dredged in cohesive material have steep sides, and high siltation rates are encouraged by flow separation.

Clearly, calculation of infill rates of dredged channels is important to the economic viability of particular engineering schemes, and many calculation methods have been suggested, varying from simplistic approaches with bulk flow parameters (4), to more recent ones, based on detailed mixing processes (2,6,10). There are, however, difficulties with some of the modern approaches, particularly for steep-sided channels. Approaches based on mixing length techniques produce unrealistic mixing parameters for sediments (2), while more advanced methods assume a spatially constant distribution of dissipation parameters for internal energy (10).

The present paper examines the use of computer methods to reproduce flow and mixing patterns in a steep-sided channel, dredged at right angles to the main direction of the flow and sediment transport.

BASIC EQUATIONS

The governing turbulent mean equations for turbulent flow over a dredged cut can be written in the form

$$\frac{\partial u}{\partial t} + u\frac{\partial u}{\partial x} + w\frac{\partial u}{\partial z} + \frac{1}{\rho}\frac{\partial p}{\partial x} - \frac{1}{\rho}\frac{\partial \tau_{zx}}{\partial z} = 0 \quad \ldots\ldots\ldots\ldots\ldots\ldots (1)$$

[1]Lect., Hydraulics Dept., School of Tech., Thessaloniki Univ., Thessaloniki, Greece.
[2]Sr. Lect., Simon Engrg. Labs., Manchester Univ., Manchester, England.

Note.—Discussion open until January 1, 1982. To extend the closing date one month, a written request must be filed with the Manager of Technical and Professional Publications, ASCE. Manuscript was submitted for review for possible publication on November 13, 1979. This paper is part of the Journal of the Hydraulics Division, Proceedings of the American Society of Civil Engineers, ©ASCE, Vol. 107, No. HY8, August, 1981. ISSN 0044-796X/81/0008-0989/$01.00.

$$\frac{\partial w}{\partial t} + u\frac{\partial w}{\partial x} + w\frac{\partial w}{\partial z} + \frac{1}{\rho}\frac{\partial p}{\partial z} - \frac{1}{\rho}\frac{\partial \tau_{xz}}{\partial x} = -g \quad \ldots\ldots\ldots\ldots\ldots\ldots (2)$$

$$\frac{\partial u}{\partial x} + \frac{\partial w}{\partial z} = 0 \quad \ldots\ldots\ldots\ldots\ldots\ldots\ldots\ldots\ldots\ldots (3)$$

using the notation of Fig. 1, in which u, w = flow velocities in the x and z directions, respectively; ρ = the fluid density; g = the acceleration due to gravity; p = the pressure in the fluid; and $\tau_{xz} = \tau_{zx}$ = an equivalent turbulent shear stress in the horizontal plane. Other stress gradients have been neglected in comparison with the τ_{zz} term.

Integration of Eq. 2, with respect to z, shows that the pressure within the fluid depends upon the density of the fluid, and the mean and turbulent characteristics of the flow field. However, in most river and marine situations,

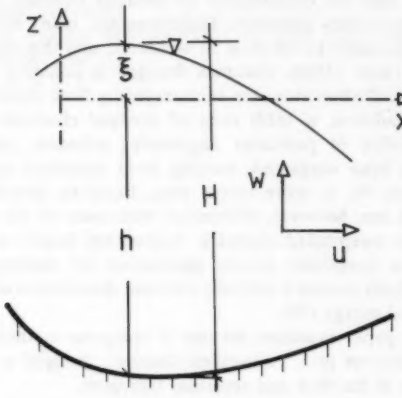

FIG. 1.—Basic Notation of Model

channel side slopes are such that only the density factor is significant even when channel side slopes are steep. The pressure distribution with depth in the present work is thus taken to be hydrostatic as a first approximation. The computer methods presented can, however, be used iteratively, if required, to include both density and flow field nonuniformity.

Eqs. 1–3 after the drop of the vertical momentum term may be rewritten in the form

$$\frac{\partial u}{\partial t} = L(u) + \alpha \quad \ldots\ldots\ldots\ldots\ldots\ldots\ldots\ldots\ldots\ldots (4a)$$

$$\text{in which} \quad L(u) = -u\frac{\partial u}{\partial x} - \frac{\partial}{\partial z}\left(\frac{\tau_{zx}}{\rho}\right) \quad \ldots\ldots\ldots\ldots\ldots\ldots (4b)$$

$$\alpha = -g\frac{\partial \xi}{\partial x} \quad \ldots\ldots\ldots\

$$f(\eta) = -3\eta(3\eta - 2) \quad \text{for} \quad \eta \leq \frac{1}{3} \quad \ldots\ldots\ldots\ldots\ldots\ldots \quad (11a)$$

$$f(\eta) = 1 \quad \text{for} \quad \eta > \frac{1}{3} \quad \ldots\ldots\ldots\ldots\ldots\ldots\ldots\ldots \quad (11b)$$

Boundary conditions are required at:

1. The water surface, $\eta = 1$. A zero velocity gradient ($\partial u/\partial z = 0$) is assumed, in the absence of surface wind, implying zero shear stress ($\tau_{zx} = 0$). The zero gradient is used ($\partial k/\partial z = 0$) (7) for the k equation.
2. The channel bed ($\eta = 0$). A nonslip condition is used, $u = 0$ for simplicity. This applies at a height η_0 ($\eta_0 = z_0/H$) equal to the equivalent bed roughness height (z_0), according to logarithmic equation, Eq. 18. The computer method thus implicitly contains an η_0 value related to discretization. A $k = 0$ condition is also used in preference to a somewhat arbitrarily specified value at η_0 (7).
3. Upstream boundary. A specified velocity profile just upstream of the dredged channel section is used.
4. Downstream boundary. A nonreflection condition is used given by

$$UH = \xi\sqrt{gH} \quad \ldots\ldots\ldots\ldots\ldots\ldots\ldots\ldots\ldots\ldots \quad (12)$$

Solution Method

Eqs. 4–11 are solved by a mixed finite-difference/finite-element procedure (3). A splitting technique is used in time to reduce the dimensionality of the problem while a one-dimensional Galerkin finite-element approach is used over the flow depth to minimize numerical errors and enable complex bed geometry to be handled on a routine basis.

The splitting technique (11) consists of dividing the differential operators of Eqs. 4 and 9 into two parts

$$L(u) = L_1(u) + L_2(u) \quad \ldots\ldots\ldots\ldots\ldots\ldots\ldots\ldots \quad (13a)$$

in which $$L_1 = -u\frac{\partial}{\partial x} \quad \ldots\ldots\ldots\ldots\ldots\ldots\ldots\ldots \quad (13b)$$

$$L_2 = \frac{\partial}{\partial z}\left(\nu_e \frac{\partial}{\partial z}\right) \quad \ldots\ldots\ldots\ldots\ldots\ldots\ldots\ldots \quad (13c)$$

Eqs. 4 and 9 can thus be integrated numerically from time level $t = n\Delta t$ to time level $t = (n + 1)\Delta t$ in two steps

$$\frac{u^* - u^n}{\Delta t} + u^n\frac{\partial u^n}{\partial x} + g\frac{\partial \xi^{n+1/2}}{\partial x} = 0 \quad \ldots\ldots\ldots\ldots\ldots\ldots \quad (14a)$$

$$\frac{u^{n+1} - u^*}{\Delta t} - \frac{\partial}{\partial z}\left(\nu_e^n \frac{\partial u^{n+1}}{\partial z}\right) = 0 \quad \ldots\ldots\ldots\ldots\ldots\ldots \quad (14b)$$

$$\frac{k^* - k^n}{\Delta t} + u^n\frac{\partial k^n}{\partial x} - \nu_e^n\left(\frac{\partial u^n}{\partial z}\right)^2 + \frac{c_d(k^n)^{3/2}}{L_0} = 0 \quad \ldots\ldots\ldots\ldots \quad (14c)$$

$$\frac{k^{n+1} - k^*}{\Delta t} - \frac{\partial}{\partial z}\left(\nu_\sigma^n \frac{\partial k^{n+1}}{\partial z}\right) = 0 \quad \ldots\ldots\ldots\ldots\ldots\ldots\ldots\ldots \quad (14d)$$

A leap-frog scheme is used for successive computations of u and ξ, and allows the use of $\xi^{n+1/2}$ values during the computation of u^{n+1}. Model time steps are controlled by the explicit steps, Eqs. 14*a* and 14*c*, and require that

$$\Delta t \leq \frac{\Delta x}{(gH)^{0.5}} \quad \ldots\ldots\ldots\ldots\ldots\ldots\ldots\ldots\ldots\ldots\ldots\ldots\ldots\ldots \quad (15)$$

in which Δx = the minimum space step used in the computations.

The water depth at each flow cross section is divided into a constant number of finite elements, as shown in Fig. 2. The velocity and turbulent kinetic energy functions are approximated by the series

$$\phi = \sum_{i=1}^{M} [N]_i \{\phi\}_i \quad \ldots\ldots\ldots\ldots\ldots\ldots\ldots\ldots\ldots\ldots\ldots\ldots\ldots \quad (16)$$

in which the summation is taken over the M elements of each cross section; $[N]_i$ = matrix of shape functions for element (i); and $\{\varphi\}_i$ = a vector

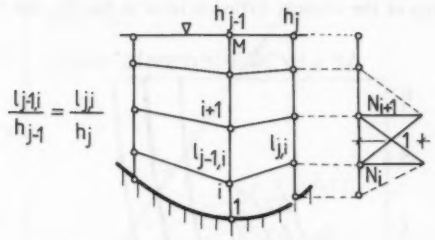

FIG. 2.—Discretization of Flow Field

of nodal u and k values. Substitution of Eq. 16 into Eq. 14 leads to the appearance of residuals, R, which are minimized by the Galerkin approach,

$$\int_{l_i} R_j N_\alpha \, dz = \int_{l_i} (\text{Eq. j}) \, N_\alpha \, dz = 0 \quad \ldots\ldots\ldots\ldots\ldots\ldots\ldots\ldots \quad (17)$$

in which $\alpha = i, i + 1$; Eq. j denotes Eqs. 14*a*, 14*b*, 14*c*, or 14*d*. The use of linear-shape functions in Eq. 17 leads to a set of equations for the unknown u and k values over the flow depth at each cross section.

Derivative terms appearing in Eq. 17 are replaced by central finite-difference expressions, and the total set of equations is solved iteratively using a Gauss-Seidel approach. Rapid convergence is found, and computation times are kept low.

Determination of λ_m, λ_0 Factors

In a steady uniform flow, it is possible to derive analytical expressions for

λ_m and λ_0 by assuming a velocity profile over the flow depth. If a logarithmic form is used, e.g., according to

$$u = \frac{u_*}{\kappa} \ln\left(\frac{\eta}{\eta_0}\right) \quad \ldots \quad (18)$$

in which $u_* = \sqrt{\tau_b/\rho}$, where τ_b = the bed shear stress; and κ = von Karman's constant; and λ_m and λ_0 are related by equations

$$\lambda_m = c_d^{-1/4} \lambda_0 \quad \ldots \quad (19a)$$

$$\text{with} \quad \lambda_m = \kappa \quad \ldots \quad (19b)$$

Analytical expressions for $f(\eta)$, ν_e, and k are also known, once u is specified, namely

$$f(\eta) = \eta(1-\eta)^{1/2} \quad \ldots \quad (20)$$

$$\nu_e = -\kappa H u_* \eta(1-\eta) \quad \ldots \quad (21)$$

$$k = -u_*^2 c_d^{-0.5}(1-\eta) \quad \ldots \quad (22)$$

As the k and, consequently, the $f(\eta)$ analytical distributions, Eqs. 20–22, are based on the drop of the vertical diffusion term in Eq. 9*b*, the $f(\eta)$ distribution

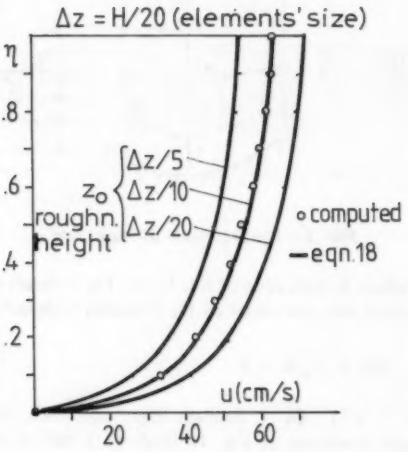

FIG. 3.—Determination of Roughness Height Implied by Numerical Integration; Uniform Flow

given by Eq. 11 will be used in this work. In order to use this $f(\eta)$ distribution in the computer solution, it is necessary to minimize the difference between Eqs. 7, 8, 10, and 21 and thus determine values of λ_m and λ_0. One way of achieving this minimization is by equating depth-mean differences to zero, i.e., for the mixing length model

$$\int_{-h}^{\epsilon} \left[l_m^2 \left| \frac{\partial u}{\partial z} \right| - \kappa u_* \frac{z(z+H)}{H} \right] dz$$

$$= \int_{-h}^{\epsilon} \left[\frac{f(\eta)^2 \lambda_m^2 H^2 u_*}{\kappa(z+H)} - \kappa u_* \frac{z(z+H)}{H} \right] dz = 0 \quad \ldots\ldots\ldots\ldots\ldots (23)$$

which leads to a λ_m value of 0.125. A similar equation for the TKE model gives a λ_0 value of 0.085. A check on the accuracy of the proposed minimization

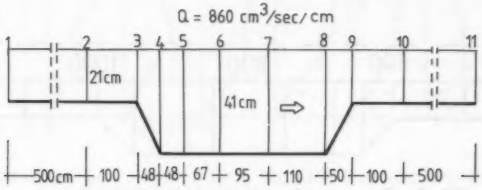

FIG. 4.—Real Flow Field and Its Discretization

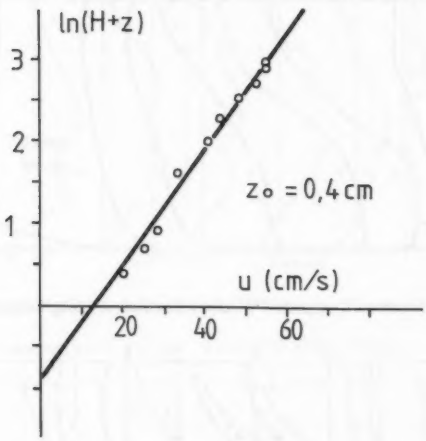

FIG. 5.—Determination of Flume Roughness Height from Velocity Profile of Uniform Flow

method was provided by operating the computer model with the calculated λ_m, λ_0 values and comparing the velocity distribution obtained with Eq. 18. Fig. 3 shows an example of this comparison. Use of Eq. 18 also enables determination of the roughness height implied by the computer model solved from the bottom ($u = 0$) to the surface. Numerical tests with equally spaced elements showed that, for the mixing length closure, the implicit z_0 was found to be one-tenth the length of the elements. A value of one-fifth of the elements' length was found for the k closure.

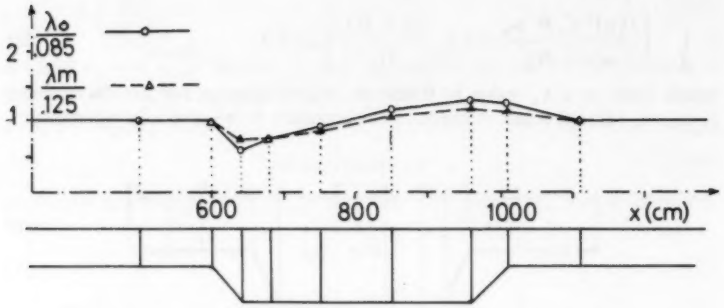

FIG. 6.—Computed Longitudinal Variations of λ_o, λ_m

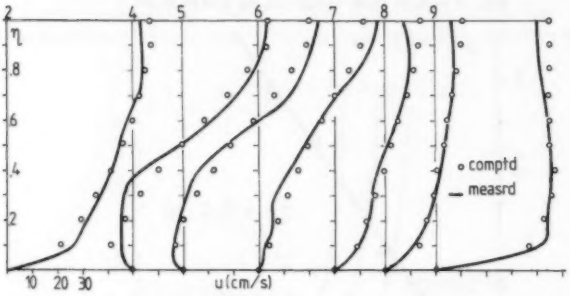

FIG. 7.—Measured Versus Computed Velocity Profiles; Mixing Length Closure

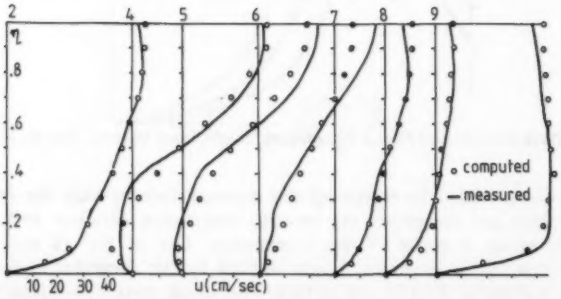

FIG. 8.—Measured Versus Computed Velocity Profiles; TKE Closure

In nonuniform flow, the λ_m and λ_0 factors vary spatially, and ideally, a two-equation turbulence closure should be used. However, at a first approxima-

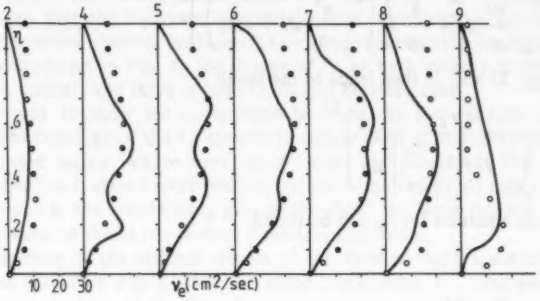

FIG. 9.—Measured Versus Computed Eddy Viscosity Distributions; Mixing Length Closure

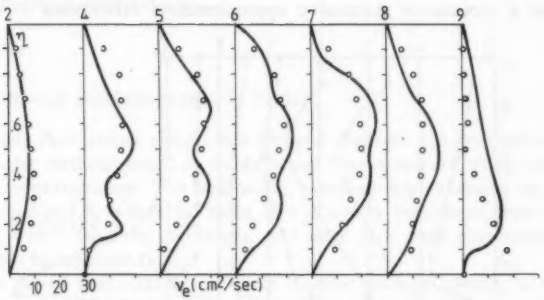

FIG. 10.—Measured Versus Computed Eddy Viscosity Distributions; TKE Closure

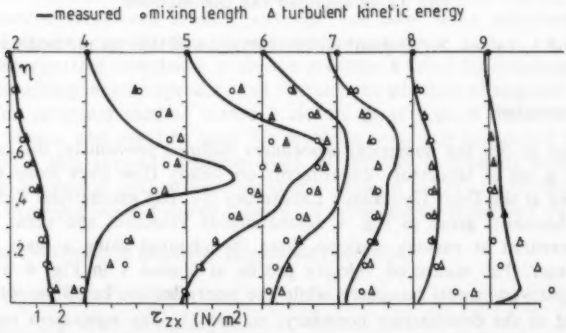

FIG. 11.—Measured Versus Computed Shear Stresses

tion, the aforementioned approach can be used, provided that u_* is adjusted locally. Integration of Eq. 4*a* over the flow mean depth leads to the result

$$u_* = \left[\int_{-h}^{0} \frac{\partial u}{\partial t} dz + \frac{\partial}{\partial x} \left(\int_{-h}^{0} \frac{u^2}{2} dz + gH\xi \right) \right]^{0.5} \quad \ldots\ldots\ldots\ldots (24)$$

Use of Eqs. 23 and 24 then leads to the result

$$\lambda_m = \left[\frac{\kappa u_*}{6 \int_{-h}^{0} f(z)^2 \left| \frac{\partial u}{\partial z} \right| dz} \right]^{0.5} \quad \ldots\ldots\ldots\ldots\ldots\ldots\ldots\ldots (25)$$

Similarly an equation for λ_0 can be found

$$\lambda_0 = \frac{\kappa u_*}{6 \int_{-h}^{0} f(z) k^{0.5} dz} \quad \ldots\ldots\ldots\ldots\ldots\ldots\ldots\ldots\ldots\ldots (26)$$

The u and k values for use in Eqs. 24–26 are obtained from the computer model and a process of successive approximations established to determine

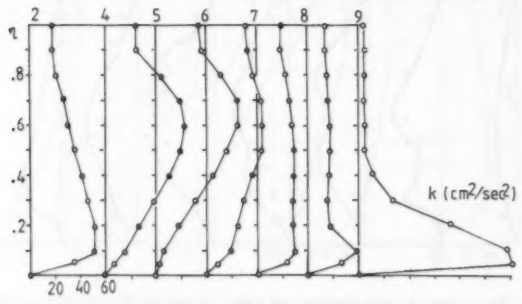

FIG. 12.—Computed TKE Distributions

the λ_m and λ_0 values. Subsequent model tests showed that the method converged rapidly.

Model Application

In order to test the numerical procedures outlined previously, use has been made of a set of laboratory experiments on steady flow over steep trenches conducted at the Delft Hydraulics Laboratory (8). The geometrical description of the channel is given in Fig. 4. Instantaneous velocities and shear stresses were measured at various stations along the channel using a laser doppler anemometer. The measured velocity profile at station 1 in Fig. 4 was used as the upstream model boundary while the nonreflection condition of Eq. 12 was used at the downstream boundary, station 11. The equivalent roughness height, z_0, of the channel was determined to be 4 mm, based on the semilogarithmic plot of the station 2 velocity data (see Fig. 5).

Eqs. 24–26 were used with the computer velocities and produced a λ_m, λ_0 variation through the channel, as shown in Fig. 6. The velocity profile associated with Fig. 6 for the mixing length closure is shown in Fig. 7, from which it can be seen that the hydrostatic approximation represents a good approach to the steep-sided channel problem. The corresponding velocity figure for the k closure is shown in Fig. 8. the degree-of-fit of both closure models is seen to be very similar, and there is little to choose between them.

Figs. 9 and 10 show the comparison between the two closure models for ν_e. The disadvantage of the l_m closure is clearly seen at stations 5 and 6, near the separated region, where very small values are predicted. The k closure, on the other hand, shows more realistic values in the separated area and slightly higher values in the accelerating part of the flow; the large surface values are a consequence of the $\partial k/\partial z$ surface boundary condition.

Reproduction of the internal details of the flow by both methods is rather similar, as shown in Fig. 11, for the shear stress term, τ_{zx}. The greatest area of discrepancy occurs on the downstream channel slope, due to the development of large k values, as shown in Fig. 12. Generally, the k closure model predicts larger τ_{zx} values than the l_m model, and has a marginally better degree-of-fit to the laboratory observations.

Conclusions

The following conclusions may be made:

1. Steady flow across steep-sided dredged channels can be predicted closely by computer methods based on fundamental flow equations, using a hydrostatic pressure approximation. The hydrostatic pressure approximation works better at stations 4 and 5, where the main flow is nearly horizontal, than at stations 8 and 9, where the flow converges, and there is a more pronounced vertical component in the main flow.
2. The mixed finite-difference/finite-element method appears to be capable of modeling both uniform and nonuniform flows at reasonable cost and with reasonable accuracy.
3. The computer method can readily be used either with mixing length or one-equation turbulence models, although the latter more advanced closure method requires considerably larger computation times.
4. One-equation turbulence, k closure provides a better fit to laboratory data than the mixing length approach, and obviates the problem of singular ν_e values.
5. The computer method with a k closure gives a good reproduction of u and ν_e values, and could be used for problems involving suspended loads, but provides a less accurate representation of internal parameters such as k or τ_{zx}. The suggested method requires modification in the $f(\eta)$ postulation or the use of two-equation turbulence closure for problems involving bed load.

Appendix I.—Details of Numerical Integration Procedure

Properties of Base Functions

$$N_i = \frac{z_{i+1} - z}{l_i}; \quad N_{i+1} = \frac{z - z_i}{L_i} \quad \ldots \ldots \ldots \ldots \ldots \ldots \ldots \ldots \quad (27)$$

$$\frac{\partial N_i}{\partial z} = -\frac{1}{l_i}; \quad \frac{\partial N_{i+1}}{\partial z} = \frac{1}{l_i} \quad \ldots\ldots\ldots\

A similar approach to the aforementioned leads to the turbulent kinetic energy equations

$$[C]\{k\}^* = \{c\} \quad \ldots \quad (39)$$

$$[D]\{k\}^{n+1} = \{d\} \quad \ldots \quad (40)$$

Typical elements of the preceding matrices are

$$C_{mj} = \int_{l_i} \frac{N_m N_j}{\Delta t}\, dz = A_{mj} \quad \ldots \quad (41)$$

$$c_m = \int_{l_i} \left[\frac{N_e k_e^n}{\Delta t} N_m - N_e u_e^n \frac{\partial}{\partial x}(N_p k_p^n) N_m + N_p v_{ep}^n \left(\frac{\partial}{\partial z} N_e u_e^n \right)^2 - c_m N_p \frac{k_p^n}{L_{0p}} \right] N_m \quad \ldots \quad (42)$$

$$B_{mj} = D_{mj} = \int_{l_i} \left(\frac{N_m N_j}{\Delta t} 1\, N_p v_{ep}^n \frac{\partial N_m}{\partial z} \frac{\partial N_j}{\partial z} \right) dz \quad \ldots \quad (43)$$

$$d_m = \int_{l_i} \frac{N_p k_p^{n+1}}{\Delta t} N_m\, dz \quad \ldots \quad (44)$$

The derivatives with respect to x of u, k, and ξ functions are replaced by central finite differences on a staggered grid (the u and k values are computed on the cross sections, and the ξ values are computed on midpoints between the two sections). The global matrices $[A]$, $[B]$, $[C]$, $[D]$, $\{a\}$, $\{b\}$, $\{c\}$, $\{d\}$ are formed by superposition of the matrix elements with the same indices (5) over a cross section. The integrations in Eqs. 33, 34, 37, 38, 41–44 are performed either analytically by the aid of Eq. 30 or numerically by the use of Gauss quadrature.

Integration of the Continuity Equation

After the computation of the u^{n+1} profiles and their depth mean values, U^{n+1}, on each cross section, the finite difference form of Eq. 5 becomes

$$\frac{\xi_{j+1/2}^{n+1/2} - \xi_{j+1/2}^{n+1/2}}{\Delta t} = -\left(\frac{U_{j+1}^{n+1} H_{j+1}^{n+1} - U_j^{n+1} H_j^{n+1}}{\Delta x} \right) \quad \ldots \quad (45)$$

Appendix II.—References

1. Huebner, K., *The Finite Element Method for Engineers*, John Wiley and Sons, Inc., New York, N.Y., 1975.
2. Kerssens, P., et al., "Model for Non Steady Suspended Sediment Transport," *Proceedings*, Seventeenth International Association for Hydraulic Research Conference, Vol. I, 1977, pp. 113–120.
3. Koutitas, C., and O'Connor, B., "Numerical Modeling of Suspended Sediments," *Advances in Water Resources*, Vol. 3, No. 2, 1980.
4. Lamblé, X., "Methode de Calcul Approchée des Ouvrages de Deconstation," *Le Houille Blanche*, Grenoble, France, 1958.
5. O'Connor, B., "Siltation in Dredged Channels," *Paper E2*, First International Symposium on Dredging Technology, 1975.

6. O'Connor, B., and Leán, G., "Estimation of Siltation in Dredged Channels in Open Situations," *Paper 2*, PIANC Congress, Leningrad, Section II, 1977.
7. Rodi, W., "Mathematical Modelling of Turbulent Diffusion in Open Channels," *Proceedings*, Euromech Colloquium 130, 1980.
8. "Semi-empirical Model for the Flow in Dredged Trenches," *Report RI267*, Delft Hydraulics Laboratory, 1979.
9. Smith, T., "A Mathematical Model for Partially Mixed Estuaries," thesis presented to Manchester University, at Manchester, England, in 1978, in partial fulfillment of the requirements for the degree of Doctor of Philosophy.
10. Smith, T., and O'Connor, B., "A Two Dimensional Model for Suspended Sediment Transport," *Proceedings*, Seventeenth International Association for Hydraulic Research Conference, Vol. I, 1977, pp. 79–86.
11. Verboom, A., "The Advective Dispersion Equation for an Anisotropic Medium Solved by the Fractional Step Method," *Mathematical Models for Environmental Problems*, C. Brebbia, ed., Pentech Press, London, England, 1975.

Appendix III.—Notation

The following symbols are used in this paper:

c_d = k turbulence closure parameter;
f = normalized mixing length or dissipation length distribution;
H = total water depth;
h = mean water depth;
k = turbulence kinetic energy;
L_0 = dissipation length parameter;
l_m = mixing length parameter;
N = shape function;
p = pressure;
R = residual function;
U = depth-mean velocity value;
u, v, w = water velocity components;
u_* = friction velocity;
$\Delta t, \Delta x$ = numerical integration steps (time, space);
η = nondimensional water depth;
κ = Von Karman constant;
λ_m, λ_0 = mixing length, dissipation length factors;
ν_e = kinematic eddy viscosity;
ξ = free surface elevation;
τ_{zx} = shear stress in turbulent flow; and
τ_b = bottom shear stress.

WATER ROUTING ON DIVERGING-CONVERGING WATERSHEDS

By Necati Ağiralioğlu[1]

INTRODUCTION

Natural watersheds have complex geometric configurations. For modeling of runoff on a natural watershed using a physically based approach, it is necessary to transform its complex geometry into a simpler one having hydrologic response. The simplified geometric representation is usually composed of some combination of three basic geometric elements: (1) Plane section (3,10); (2) converging section (13,15); and (3) diverging section (1,14).

Some watersheds, both rural and urban, are roughly leaf-shaped. Their upland portions diverge, and their lower portions converge. If a watershed is diverging and converging, then coupling of the diverging section with the converging section may be desired to represent it. This geometric representation can be called a diverging-converging configuration. The questions are: does this representation allow a better hydrograph prediction than alternative representations? And what are the effects of varying geometric parameters on the runoff hydrograph?

In this study, the overland flow equations depending on the kinematic wave theory are solved by using an implicit finite difference method for the diverging-converging configuration. This diverging-converging flow model is applied to impervious surfaces which preserve the area and the length of the watershed and fix the kinematic parameters for each event. The effects of varying geometric parameters on runoff hydrographs are investigated, and the results are compared with other geometric representations.

The geometry of a diverging-converging surface is shown in Fig. 1, in which R_1 = the length of a diverging section; L_1 = the length of flow for a diverging section; θ_1 = the radial angle for a diverging section; d = the degree of divergence; R_2 = the length of a converging section; θ_2 = the radial angle for a converging section; L_2 = the length of flow for a converging section; c = the degree of convergence; L = the total flow length; and Z = the total length of the sections. The degree of divergence, d, = a dimensionless parameter = $(R_1 - L_1)/R_1$. Also, the degree of convergence, c, = a dimensionless parameter = $(R_2 - L_2)/R_1$.

[1]Asst. Prof. of Civ. Engrg., Technical Univ. of Istanbul, Turkey.

Note.—Discussion open until January 1, 1982. To extend the closing date one month, a written request must be filed with the Manager of Technical and Professional Publications, ASCE. Manuscript was submitted for review for possible publication on July 14, 1980. This paper is part of the Journal of the Hydraulics Division, Proceedings of the American Society of Civil Engineers, ©ASCE, Vol. 107, No. HY8, August, 1981. ISSN 0044-796X/81/0008-1003/$01.00.

THEORY

The basic equations of unsteady flow in an open channel are the continuity and momentum equations. For a diverging section, the continuity equation can be written (14) as

$$\frac{\partial h}{\partial t} + \frac{\partial q}{\partial r} + \frac{q}{r} = i \quad \ldots \ldots \ldots

equation can be given as

$$S_f \simeq S_o \quad \ldots \quad (4)$$

in which S_f = the friction slope; and S_o = the bed slope. Friction slope is related to flow regime by using the Darcy-Weisbach, Chezy, or Manning formulas. In this study, the Darcy-Weisbach friction formula is used,

$$S_f = f\frac{q^2}{8gR'h^2} \quad \ldots \quad (5)$$

in which f = the friction factor; R' = the hydraulic radius; and g = the gravitational acceleration.

Based upon some investigations (2,12), the friction factor can be expressed for all practical flow regimes as

$$f = \frac{a}{\mathrm{R}^b} \quad \ldots \quad (6)$$

in which a, b = constants depending on surface characteristics; and R = the Reynolds number. Assuming $R' = h$ for a wide section, and putting $\mathrm{R} = q/\nu$, elimination of f and S_f from Eqs. 4–6 gives

$$q = \left(\frac{8gS_o}{a\nu^b}\right)^{1/2-b} h^{3/2-b} \quad \ldots \quad (7)$$

in which ν = the kinematic viscosity. For conciseness, Eq. 7 can be written

$$q = \alpha h^{\beta} \quad \ldots \quad (8)$$

in which α and β = coefficients whose value depends on the roughness of the channel and the friction slope. Thus, for the kinematic wave approximation, the momentum equation becomes a discharge-depth relationship.

The substitution of Eq. 8 into Eq. 1 gives

$$\frac{\partial h}{\partial t} + \alpha\beta h^{\beta-1}\frac{\partial h}{\partial r} + \frac{\partial h^{\beta}}{r} = i \quad \ldots \quad (9)$$

This is the kinematic wave equation for diverging flow. Similarly, Eq. 2 yields the kinematic wave equation for converging flow as

$$\frac{\partial h}{\partial t} + \alpha\beta h^{\beta-1}\frac{\partial h}{\partial r} - \frac{\alpha h^{\beta}}{Z-r} = i \quad \ldots \quad (10)$$

To calculate the flow from a diverging-converging watershed, Eqs. 9 and 10 can be orderly solved on diverging and converging sections for boundary and initial conditions. For a diverging section, the boundary condition is $h = 0$ when $r = dR_1$. The assumption of the downstream width of a diverging section equal to the upstream width of a converging section results in the boundary condition of a converging section equal to the downstream condition of a diverging section, which, in turn, results from the computation of the first section. Therefore, for a converging section, the upstream depth may be equal to the downstream depth of a diverging section. Initial conditions are the same for both sections as $h = 0$ when $t = 0$.

For different geometric configurations, it is more useful to compare the discharge values instead of q. The discharge can be expressed as $Q = q\,B_2$, in which Q = the discharge; and B_2 = the width of the watershed outlet. Therefore, the computation of the discharge values requires the determination of the outlet width which can be estimated from other geometric parameters.

The area of the diverging section can be written as

$$A_1 = \frac{2\pi R_1(1 - d^2)\theta_1}{360} \quad \ldots\ldots\ldots\ldots\ldots\ldots\ldots\ldots\ldots\ldots\ldots\ldots \quad (11)$$

in which A_1 = the area of a diverging section. The downstream width of this section is

$$B_1 = \frac{2\pi R_1\theta_1}{360} \quad \ldots\ldots\ldots\ldots\ldots\ldots\ldots\ldots\ldots\ldots\ldots\ldots\ldots\ldots \quad (12)$$

in which B_1 = the downstream width of a diverging section. Setting $L_1 = R_1(1 - d)$ and eliminating θ_1 from Eqs. 11 and 12 gives

$$B_1 = \frac{2A_1}{L_1(1 + d)} \quad \ldots\ldots\ldots\ldots\ldots\ldots\ldots\ldots\ldots\ldots\ldots\ldots\ldots\ldots \quad (13)$$

Assuming that the downstream width of a diverging section is equal to the upstream width of a converging section, the upstream width of converging a section can be written as

$$B_1 = \frac{2A_2}{L_2(1 + c)} = \frac{2A}{L\,[\rho(1 + d) + (1 - \rho)(1 + c)]} \quad \ldots\ldots\ldots\ldots\ldots \quad (14)$$

in which A_2 = the area of converging section; $A = A_1 + A_2$ = the total watershed area; and $\rho = L_1/L$. Similarly, the outlet width can be expressed

$$B_2 = \frac{2cA_2}{L_2(1 + c)} = \frac{2cA}{L\,[\rho(1 + d) + (1 - \rho)(1 + c)]} \quad \ldots\ldots\ldots\ldots\ldots \quad (15)$$

Because of radial symmetry, θ_1 and θ_2 do not enter explicitly into the computation. Thus, for preserving watershed area and length, there are only three geometric parameters, c, d, and ρ, which enter into the computation. These dimensionless parameters assume values between 0 and 1 depending on watershed geometry. For some special values of these parameters, the diverging-converging configuration gives some other idealistic geometric representations as shown in Table 1. These six geometric configurations will represent most natural watersheds.

Numerical Method

Explicit and implicit finite difference methods have been used successfully in many investigations on kinematic wave modeling of watershed runoff (1,4,6). Although explicit schemes are simple to formulate and are easy to program, they are conditionally stable. However, the implicit schemes are considerably more difficult to program than explicit schemes, and they are theoretically

unconditionally stable in a linear sense. But they also have some practical limitations in stability.

Ağiralioğlu and Singh (1) used first-order and second-order explicit schemes for diverging and rectangular sections. But these schemes were not stable for converging sections, especially for small values of degree of convergence. Herein, a four-point implicit scheme is used for numerical solutions. Any dependent

TABLE 1.—Geometric Parameters for Diverging-Converging Model and for Its Special Cases

Geometric representation (1)	Geometric Parameters: Length ratio, $\rho = L_1/L$ (2)	Degree of divergence, $d = (R_1 - L_1)/R_1$ (3)	Degree of convergence, $c = (R_2 - L_2)/R_2$ (4)
Diverging-converging	$0 < \rho < 1$	$0 \le d < 1$	$0 < c < 1$
Diverging-rectangular	$0 < \rho < 1$	$0 \le d < 1$	$c = 1$
Rectangular-converging	$0 < \rho < 1$	$d = 1$	$0 < c < 1$
Diverging	$\rho = 1$	$0 \le d < 1$	
Converging	$\rho = 0$		$0 < c < 1$
Rectangular		$d = 1$	$c = 1$

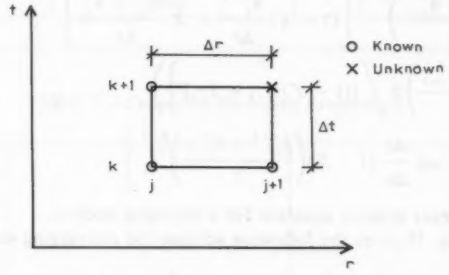

FIG. 2.—Definition Sketch for Implicit Scheme

variable, $f(r,t)$, and its partial derivatives can be approximated with four-point implicit finite differences as follows (see Fig. 2)

$$f(r,t) = (1 - X)[(1 - Y)f_{j+1}^{k+1} + Y(f_j^{k+1})] + X[(1 - Y)f_{j+1}^{k} + Y(f_j^{k})] \quad (16)$$

$$\frac{\partial f(r,t)}{\partial r} = (1 - X)\frac{f_{j+1}^{k+1} - f_j^{k+1}}{\Delta r} + X\frac{f_{j+1}^{k} - f_j^{k}}{\Delta r} \quad (17)$$

$$\frac{\partial f(r,t)}{\partial t} = (1 - Y)\frac{f_{j+1}^{k+1} - f_{j+1}^{k}}{\Delta t} + Y\frac{f_j^{k+1} - f_j}{\Delta t} \quad (18)$$

in which X = the space-weighting factor; and Y = the time-weighting factor, in which $0 \le X \le 1$ and $0 \le Y \le 1$; and Δr and Δt = space and time increments, respectively.

Since the space coordinate, r, varies only in space, the following expression holds for all values of j

$$r_j^{k+1} = r_j^k = r_j \quad \ldots \quad (19)$$

Similarly, assuming the rainfall excess is only time-variant but spatially uniform, the following expression can be written for all values of k

$$i_{j+1}^k = i_j^k = i^k \quad \ldots \quad (20)$$

Since the linear scheme, which is a good approximation of overland flow (4), provides some simplification in programming and saves computer time, a linear routing method is used. It must be noted, however, that the linear scheme requires more care in selecting Δt than a nonlinear scheme. In the linear routing method, the term h can be expressed in the following finite difference form

$$h = \frac{h_j^{k+1} + h_{j+1}^k}{2} \quad \ldots \quad (21)$$

Substitution of Eqs. 19, 20 and 21 into Eq. 9 yields

$$h_{j+1}^{k+1} = \left((1 - Y)h_{j+1}^k - Y(h_j^{k+1} - h_j^k) + \Delta t \left\{ (1 - X)i^{k+1} + Xi^k \right.\right.$$
$$+ \alpha\beta \left(\frac{h_j^{k+1} + h_{j+1}^k}{2} \right)^{\beta - 1} \left[(1 - X) \frac{h_j^{k+1}}{\Delta r} - X \frac{h_{j+1}^k - h_j^k}{\Delta r} \right]$$
$$\left.\left. - \alpha \left(\frac{h_j^{k+1} + h_{j+1}^k}{2} \right) \beta \Big/ [(1 - Y)r_{j+1} + Yr_j] \right\} \right)$$
$$\Big/ \left[(1 - Y) + \alpha\beta \frac{\Delta t}{\Delta r} (1 - X) \left(\frac{h_j^{k+1} + h_{j+1}^k}{2} \right)^{\beta - 1} \right] \quad \ldots \quad (22)$$

which is the linear scheme equation for a diverging section.

Similarly, Eq. 10 gives the following scheme for converging section

$$h_{j+1}^{k+1} = \left((1 - Y)h_{j+1}^k - Y(h_j^{k+1} - h_j^k) + \Delta t \left\{ (1 - X)i^{k+1} + Xi^k \right.\right.$$
$$+ \alpha\beta \left(\frac{h_j^{k+1} + h_{j+1}^k}{2} \right)^{\beta - 1} \left[(1 - X) \frac{h_j^{k+1}}{\Delta r} - X \frac{h_{j+1}^k - h_j^k}{\Delta r} \right]$$
$$\left.\left. + \alpha \left(\frac{h_j^{k+1} + h_{j+1}^k}{2} \right)^{\beta} \Big/ [Z - (1 - Y)r_{j+1} - Yr_j] \right\} \right)$$
$$\Big/ \left[(1 - Y) + \alpha\beta \frac{\Delta t}{\Delta r} (1 - X) \left(\frac{h_j^{k+1} + h_{j+1}^k}{2} \right)^{\beta - 1} \right] \quad \ldots \quad (23)$$

Applications

The kinematic diverging-converging model is applied to three events on

impervious surfaces which are selected from the literature (5,7,9). The general characteristics of each overland surface and its source are given in Table 2, in which B = the width of watershed; and T = the rainfall duration.

The kinematic parameters, α and β, are estimated from the reported data. For example, Morgali specified $b = 1.0$ and $a = 36.3$ for the rising hydrograph

TABLE 2.—Characteristics of Selected Events

Serial number (1)	Reference (2)	Original test number (3)	Paved type (4)	Width B, in meters (5)	Length L, in meters (6)	Slope, S_o (7)	Rainfall in density, i, in meters per hour (8)	Rainfall duration, T, in seconds (9)
1	Morgali (1970)	56	Asphalt	1.830	7.320	0.01000	0.100	300
2	Langford and Turner (1973)	43	Bitumen	4.572	22.860	0.01000	0.060	840[a]
3	Muzik (1973)	1	Galvanized sheet	0.610	0.914	0.20971	0.115	50

[a]Assumed.

TABLE 3.—Estimated Kinematic Parameters

Serial number (1)	Kinematic viscosity, ν, in millions of square meters per second (2)	Parameters for Rising Hydrograph				Parameters for Recession Hydrograph			
		a (3)	b (4)	α (5)	β (6)	a (7)	b (8)	α (9)	β (10)
1	1.30	36.30	1.00	16,630.64	3.00	32.00	1.00	18,865.38	3.00
2	1.14	5.40	0.24	2.16	1.70	76.60	0.75	94.20	2.40
3	1.00	32.00	1.00	509,899.28	3.00	24.00	1.00	679,865.70	3.00

and $a = 32.0$ for the recession hydrograph. In this case, $\beta = 3$ and $\alpha = 16630.64$ for the rising hydrograph and $\alpha = 18865.38$ for the recession hydrograph for $\nu = 1.3 \times 10^{-6}$ m^2/s. These kinematic parameters are indicated in Table 3. All computations depend on the assumption of constant kinematic parameters for different geometric representations. This assumption may be reasonable

because the kinematic parameters are related to flow regime but not to geometric parameters, except bottom slope as seen from Eqs. 7 and 8. The bottom slope is considered constant for each surface.

The weighting values, $X = 0.5$ and $Y = 0.5$, were used for all computations. For the accuracy of the results, Δr should be small, and for the achievement

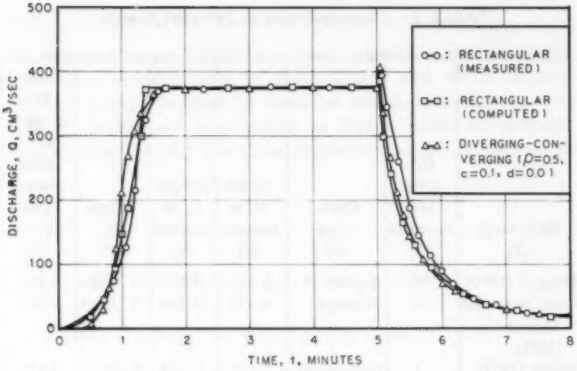

FIG. 3.—Comparison of Measured and Computed Hydrographs

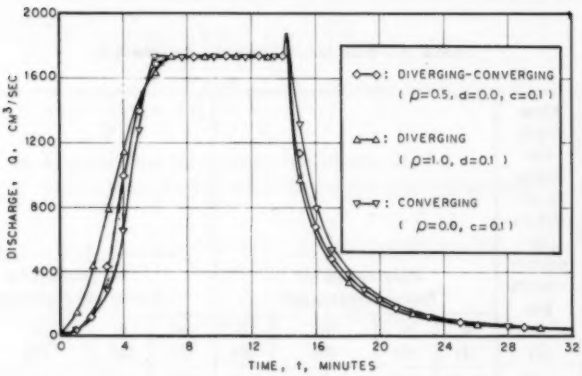

FIG. 4.—Comparison of Hydrographs for Different Geometric Representations

of the stability in practice, $\Delta t / \Delta r$ should be smaller than a certain limit. Therefore, the space interval was selected as one-fortieth of the flow length, $\Delta r = L/40$. The time interval was selected, and set at 2.0 sec, 0.5 sec, and 0.2 sec for Langford and Turner's, Morgali's, and Muzik's data, respectively. Larger values of Δt have been tested, but they have given results which deviated from the expected values for equilibrium condition.

The hydrograph obtained from Morgali's data for a diverging-converging configuration for $\rho = 0.5$, $d = 0.0$, and $c = 0.1$ is compared with the observed hydrograph and the computed hydrograph for a rectangular section as shown

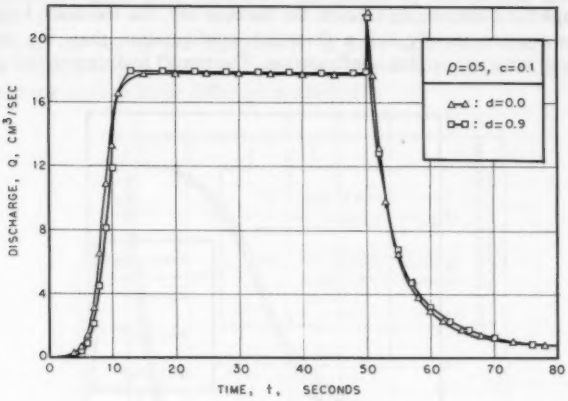

FIG. 5.—Effect of Degree of Divergence on Equilibrium Hydrograph for Diverging-Converging Model

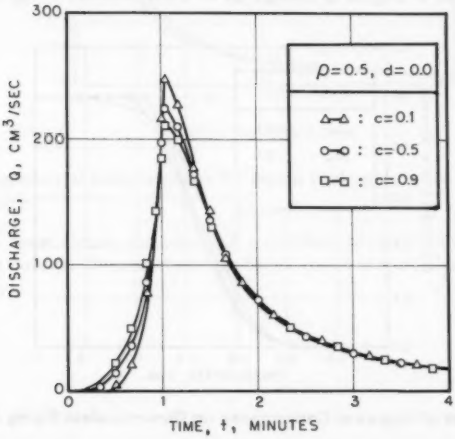

FIG. 6.—Effect of Degree of Convergence on Partial Equilibrium Hydrograph for Diverging-Converging Model

in Fig. 3. There is a good agreement between the equilibrium measured and computed discharges. This indicates that the implicit scheme with a linear routing is a good approximation for the computations.

Fig. 4 shows the effect of watershed geometry on the runoff hydrograph with Langford and Turner's figures for diverging-converging, diverging, and converging configurations. As seen from this figure, the rising hydrograph for a diverging configuration goes up more rapidly in the beginning than the rising hydrograph for a converging section. On the contrary, the recession hydrograph goes down more rapidly for a diverging configuration than the recession hydrograph for a converging configuration. The runoff hydrograph for a diverg-

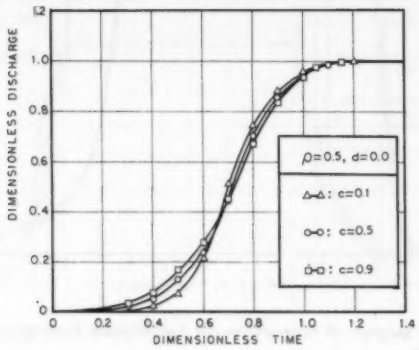

FIG. 7.—Effect of Degree of Divergence on Dimensionless Rising Hydrograph

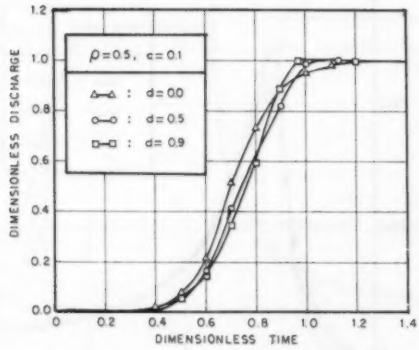

FIG. 8.—Effect of Degree of Convergence on Dimensionless Rising Hydrograph

ing-converging configuration stays between the values of these two configurations. On the other hand, the diverging representation gives the longest time of concentration.

Fig. 5 shows the effect of degree of divergence, d, on the runoff hydrograph for Muzik's data. In this case, the hydrographs do not change significantly as the value of d increases.

To obtain a partial equilibrium hydrograph, the rainfall duration, T, was selected as 60 sec for Morgali's data. For this case, the effect of the degree of convergence, c, on the runoff hydrograph is given in Fig. 6. This figure shows that the peak discharge varies with geometric parameters in the partial equilibrium condition.

In general, the results are found to be in good agreement with a previous study, in which diverging and rectangular flows were investigated on impervious surfaces using explicit finite different methods (1).

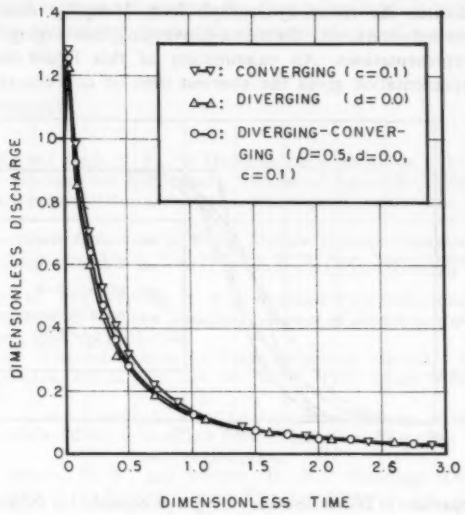

FIG. 9.—Comparison of Dimensionless Recession Hydrographs for Different Watershed Geometries

In order to show clearly the effect of watershed geometry both on the rising and recession curves, dimensionless discharge and time variables are designated with asterisks

$$Q_* = \frac{Q}{Q_o}; \quad \ldots \quad (24)$$

$$t_* = \frac{t}{T_o} \quad \ldots \quad (25)$$

in which Q_o = the normalizing discharge which equals the equilibrium discharge, iA; and T_o = the normalizing time which equals the time of concentration for rectangular section, i.e., $[(L/\alpha)^{1/n} i^{(1-n)/n}]$.

Fig. 7 shows the dimensionless rising curves for different values of d, including 0.0, 0.5, and 0.9 for $\rho = 0.5$ and $c = 1.0$. This figure indicates more clearly the effect of d on the rising hydrograph than Fig. 5.

Fig. 8 shows a number of dimensionless rising hydrographs from Morgali's for different values of c, 0.1, 0.5, and 0.9, for $d = 0.0$ and $\rho = 0.5$. In a diverging-converging configuration, the parameter c is efficient in influencing the shape of hydrograph, but has little influence on the time of concentration.

Fig. 9 shows the effect of the parameter, ρ, on the recession hydrograph from Muzik's data. As seen from this figure, the recession hydrographs go down more rapidly for larger values of ρ than recession hydrographs for smaller values of ρ. The diverging configuration ($\rho = 1.0$) can give a smaller lag time than the others. Fig. 4 supports this conclusion, also.

Fig. 10 indicates the rising hydrograph from Morgali's data for different geometric representations, viz., diverging-converging, converging, diverging, and rectangular representations. An examination of this figure shows that the converging representation gives the shortest time of concentration, while the

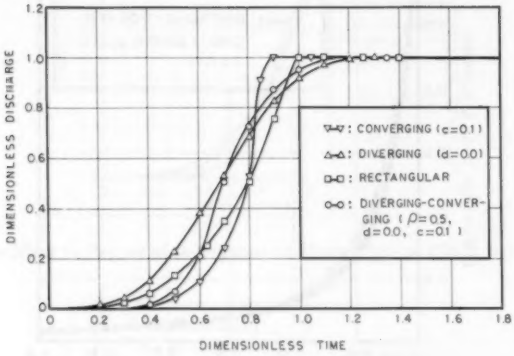

FIG. 10.—Comparison of Dimensionless Rising Hydrographs for Different Watershed Geometries

diverging representation gives the longest one. The time of concentration for the rectangular representation stays between the values of these two representations.

Conclusions

Based on the numerical study of kinematic flow equations, the following conclusions are drawn:

1. In a diverging-converging surface, the geometric parameters are important factors on both rising and recession hydrographs. A diverging-converging flow model gives hydrograph values between values of diverging and converging model depending on geometric parameters. For some special values of geometric parameters, diverging-converging models can be used for other idealistic geometric representations.
2. Different geometric representations give runoff hydrographs with different shapes under the same conditions. A comparison of three basic geometric

representations (diverging, rectangular, and converging) shows that a diverging representation gives the longest time of concentration, while a converging representation yields the shortest one. The reverse is true for lag time.

3. To simulate the hydrographs for a leaf-shaped watershed, a diverging-converging representation may be better than the other idealistic representations.

4. Since the stage, h, changes more slowly for a diverging representation than others, a diverging representation is the most stable. On the other hand, a converging representation is the least stable. Computation of a converging section needs small time intervals for stability, especially for small values of the degree of convergence. However, the four-point implicit method can be used successfully for various geometric representations of a watershed with large variations in stage.

Appendix I.—References

1. Ağiralioğlu, N., and Singh, V. P., "A Mathematical Investigation of Diverging Flow: 2. Numerical Solutions and Applications," *Technical Report No. MSSU-EIRS-80-4*, Engineering and Industrial Research Station, Mississippi State University, Miss., 1980, pp. 1–95.
2. Chen, C. L., "Flow Resistance in Broad Shallow Grassed Channels," *Journal of the Hydraulics Division*, ASCE, Vol. 102, No. HY3, Proc. Paper 11994, Mar., 1976, pp. 307–322.
3. Henderson, F. M., and Wooding, R. A., "Overland Flow and Groundwater Flow from a Steady Rainfall of Finite Duration," *Journal of Geophysical Research*, Vol. 69, No. 8, Apr., 1964, pp. 1531–1540.
4. Huang, Y. H., "Channel Routing by Finite Difference Method," *Journal of the Hydraulics Division*, ASCE, Vol. 104, No. HY10, Proc. Paper 14088, Oct., 1978, pp. 1379–1393.
5. Langford, D. J., and Turner, A. K., "An Experimental Study of the Application of Kinematic Wave Theory to Overland Flow," *Journal of Hydrology*, Vol. 18, 1973, pp. 125–145.
6. Li, R. M., Simons, D. B., and Stevens, M. A., "Nonlinear Kinematic Wave Approximation for Water Routing," *Water Resources Research*, Vol. 11, No. 2, Apr., 1975, pp. 245–252.
7. Morgali, J. R., "Laminar and Turbulent Overland Flow," *Journal of the Hydraulics Division*, ASCE, Vol. 96, No. HY2, Proc. Paper 7075, Feb., 1970, pp. 441–460.
8. Morris, E. M., and Woolhiser, D. A., "Unsteady One-Dimensional Flow Over a Plane: Partial Equilibrium and Recession Hydrographs," *Water Resources Research*, Vol. 16, No. 2, Apr., 1980, pp. 355–360.
9. Muzik, I., "State Variable Model of Surface Runoff from a Laboratory Catchment," thesis presented to the University of Alberta, at Edmonton, Canada, in 1973, in partial fulfillment of the requirements for the degree of Doctor of Philosophy.
10. Overton, D. E., and Meadows, M. E., *Stormwater Modeling*, Academic Press, New York, N.Y., 1976, pp. 1–358.
11. Ponce, V. M., Li, R. M., and Simons, D. B., "Applicability of Kinematic and Diffusion Models," *Journal of the Hydraulics Division*, ASCE, Vol. 104, No. HY3, Proc. Paper 13635, Mar., 1978, pp. 353–360.
12. Shen, H. W., and Li, R. M., "Rainfall Effect on Sheet Flow over Smooth Surface," *Journal of the Hydraulics Division*, ASCE, Vol. 99, No. HY5, Proc. Paper 9773, May, 1973, pp. 771–792.
13. Singh, V. P., "A Nonlinear Kinematic Wave Model of Surface Runoff," thesis presented to the Colorado State University, at Fort Collins, Colo., in 1974, in partial fulfillment of the requirements for the degree of Doctor of Philosophy.
14. Singh, V. P., and Ağiralioğlu, N., "A Mathematical Investigation of Diverging Flow: 1. Analytical Solutions," *Technical Report No. MSSU-EIRS-80-3*, Engineering and Industrial Research Station, Mississippi State University, Miss., 1980, pp. 1–175.

15. Woolhiser, D. A., "Overland Flow on a Converging Surface," *Transactions*, American Society of Agricultural Engineers, Vol. 12, No. 4, 1969, pp. 460–462.

Appendix II.—Notation

The following symbols are used in this paper:

$A = A_1 + A_2$ = watershed area;
A_1 = watershed area of diverging section;
A_2 = watershed area of converging section;
a = constant;
B = average width of watershed;
B_1 = downstream width of diverging section;
B_2 = downstream width of converging section;
b = constant;
$c = (R_2 - L_2)/R_2$ = degree of convergence for converging section;
$d = (R_1 - L_1)/R_1$ = degree of divergence for diverging section;
f = Darcy-Weisbach friction factor;
g = acceleration due to gravity;
h = water depth;
i = rainfall excess;
j = space discretization index;
k = time discretization index;
$L = L_1 + L_2$ = length of flow;
$L_1 = R_1(1 - d)$ = length of diverging part of region;
$L_2 = R_2(1 - c)$ = length of converging part of region;
Q = discharge;
Q_o = normalizing discharge;
$Q_* = Q/Q_o$ = dimensionless discharge;
q = discharge per unit width;
R = Reynolds number;
R_1 = length of diverging section;
R_2 = length of converging section;
R' = hydraulic radius;
r = space coordinate;
S_f = slope of friction;
S_o = slope of bed;
T = rainfall duration;
T_o = normalizing time;
$t_* = t/T_o$ = dimensionless time;
t = time;
X = weighting factor of spatial derivative;
Y = weighting factor of temporal derivative;
$Z = R_1 + R_2$ = total length of sections;
α = routing coefficient;
β = routing coefficient;
Δr = spatial increment;
Δt = temporal increment;

θ_1 = radial angle for diverging section;
θ_2 = radial angle for converging section;
ν = kinematic viscosity of water; and
$\rho = L_1/L$ = length ratio.

DISCUSSION

Note.—This paper is part of the Journal of the Hydraulics Division, Proceedings of the American Society of Civil Engineers, ©ASCE, Vol. 107, No. HY8, August, 1981. ISSN 0044-796X/81/0008-1021/$01.00.

Discussions

Discussions may be submitted on any Proceedings paper or technical note published in any *Journal* or on any paper presented at any Specialty Conference or other meeting, the *Proceedings* of which have been published by ASCE. Discussion of a paper/technical note is open to anyone who has significant comments or questions regarding the content of the paper/technical note. Discussions are accepted for a period of 4 months following the date of publication of a paper/technical note and they should be sent to the Manager of Technical and Professional Publications, ASCE, 345 East 47th Street, New York, N.Y. 10017. The discussion period may be extended by a written request from a discusser.

The original and three copies of the Discussion should be submitted on 8-1/2-in. (220-mm) by 11-in. (280-mm) white bond paper, typed double-spaced with wide margins. The length of a Discussion is restricted to two *Journal* pages (about four typewritten double-spaced pages of manuscript including figures and tables); the editors will delete matter extraneous to the subject under discussion. If a Discussion is over two pages long it will be returned for shortening. All Discussions will be reviewed by the editors and the Division's or Council's Publications Committees. In some cases, Discussions will be returned to discussers for rewriting, or they may be encouraged to submit a paper or technical note rather than a Discussion.

Standards for Discussions are the same as those for Proceedings Papers. A Discussion is subject to rejection if it contains matter readily found elsewhere, advocates special interests, is carelessly prepared, controverts established fact, is purely speculative, introduces personalities, or is foreign to the purposes of the Society. All Discussions should be written in the third person, and the discusser should use the term "the writer" when referring to himself. The author of the original paper/technical note is referred to as "the author."

Discussions have a specific format. The title of the original paper/technical note appears at the top of the first page with a superscript that corresponds to a footnote indicating the month, year, author(s), and number of the original paper/technical note. The discusser's full name should be indicated below the title (see Discussions herein as an example) together with his ASCE membership grade (if applicable).

The discusser's title, company affiliation, and business address should appear on the first page of the manuscript, along with the *Proceedings* paper number of the original paper/technical note, the date and name of the *Journal* in which it appeared, and the original author's name.

Note that the discusser's identification footnote should follow consecutively from the original paper/technical note. If the paper/technical note under discussion contained footnote numbers 1 and 2, the first Discussion would begin with footnote 3, and subsequent Discussions would continue in sequence.

Figures supplied by the discusser should be designated by letters, starting with A. This also applies separately to tables and references. In referring to a figure, table, or reference that appeared in the original paper/technical note use the same number used in the original.

It is suggested that potential discussers request a copy of the *ASCE Authors' Guide to the Publications of ASCE* for more detailed information on preparation and submission of manuscripts.

Bayesian Frequency Analysis[a]

Discussion by Arun Kumar[2] and Rema Devi[3]

The author has proposed Bayesian regression analysis for predicting flood in order to account for uncertainties in model selection and in the evaluation of parameters from limited data. The method is illustrated by fitting two-parameter distributions (normal, log normal, and Gumbel) to observed flood data. It is, however, well-recognized that three-parameter distributions such as Pearson Type III, log Pearson Type III, and general extreme distribution functions fit better to flood data than do two-parameter distributions (5,13). In the writers' opinion, the proposed methodology has very limited applicability when the three-parameter distribution is fitted. Unlike a two-parameter distribution, construction of a probability paper for a three-parameter distribution will depend upon the coefficient of skewness observed in a sample. In other words, for a given distribution, sampling errors in the estimation of skewness will result in different probability scale papers. Even additional data may cause a change in the probability scale. Since the proposed method does not account for a change of probability scale for a given distribution, uncertainty resulting in the estimation of skewness due to sampling errors cannot be accounted for.

Gumbel, normal, and log normal distributions have been fitted to Salt Fork data and it has been pointed out that although the log normal distribution apparently shows the best fit on a probability paper, it may not be an appropriate distribution for predicting flood at large return periods. The writers feel that the conclusion derived by the author is not correct.

The goodness of fit of different distributions can be checked by comparing the observed and predicted values at various return periods. The data is considered to follow that distribution which gives the closest fit (5,12). The comparative goodness of fit of Salt Fork data using the normal, the log normal, and the Gumbel distribution is given in Table 6. It is observed from the table that the log normal distribution gives a better fit as compared to the normal and the Gumbel distribution, because it has the least-mean square error and largest correlation coefficient.

The log normal distribution assumes apriori that the logarithm of flows follow a normal distribution. This may not be true in all cases. In such cases, the goodness of fit can further be improved by using a data-based power transformation (11), which reconstitutes the data such that the transformed series follows a normal distribution. This transformation which is given as

[a]July, 1980, by Wilson H. Tang (Proc. Paper 15532).

[2]Asst. Prof. of Civ. Engrg., Delhi Coll. of Engrg., Kashmere Gate, Delhi, 110006, India.

[3]Asst. Prof. of Civ. Engrg., Indian Inst. of Tech., New Delhi, India.

$$Z_i = \frac{Y_i^{\lambda} - 1}{\lambda} \quad \lambda \neq 0; \quad Z_i = \ln Y_i \quad \lambda = 0 \quad \ldots\ldots\ldots\ldots\ldots\ldots \quad (42)$$

transforms the original series, Y_i, into an approximately normal series, Z_i, for some value of λ. It can be seen from Eq. 42 that log normal is a special case of power transformation. For Salt Fork data, when $\lambda = -0.14$, the mean, standard deviation, skewness, and kurtosis of the transformed series, Z_i, are 4.7533941, 0.1769088, −0.0015, and 3.5, respectively. Taking the transformed series as normal, the flood peaks at various return periods are calculated and given in Table 6. It is observed that the power transformation gives even a better fit than does the log normal distribution. The 20-yr flood using the power transformation is 7,047 with a standard deviation of 1,155.

TABLE 6.—Observed and Fitted Flood Peaks at Salt Fork (17 yr) Using Various Models, in cubic feet per second

Observed flows (1)	Fitted Flows			
	Normal (2)	Gumbel (3)	Log normal (4)	Power transformation (5)
6,860	5,660	6,382	6,507	6,806
6,030	5,016	5,312	5,222	5,312
5,380	4,579	4,665	4,497	4,510
3,370	4,229	4,185	3,989	3,967
2,990	3,927	3,807	3,597	3,556
2,750	3,653	3,481	3,275	3,226
2,640	3,397	3,193	3,000	2,949
2,630	3,151	2,931	2,758	2,708
2,600	2,911	2,687	2,541	2,494
2,350	2,670	2,454	2,340	2,299
2,340	2,425	2,229	2,151	2,117
2,300	2,168	2,005	1,971	1,945
1,920	1,895	1,777	1,794	1,778
1,800	1,592	1,540	1,618	1,613
1,350	1,242	1,280	1,435	1,443
1,230	805	978	1,236	1,258
950	162	572	992	1,034

Note: For $\sigma = \sqrt{1/(n-1)\,\Sigma(\text{obsolete} - \text{fitted})^2}$, the values for the various fitted flows are 683, 496, 428, and 254, respectively. For the correlation coefficient, the values are 0.911, 0.954, 0.973, 0.977, respectively.

The author seems to infer that the normal distribution, which has less of a standard deviation should be preferred in comparison to the log normal and the power transformation for the estimation of a flood at a large return period. The standard deviation, as given in Eq. 18, depends upon the type of distribution chosen. It can be an index for selecting a distribution only when all the competing distributions fit the data equally well. In the writers' opinion, since the variation in the Salt Fork data is more accurately expressed by the log normal and the power transformation, the extrapolation of a flood should be estimated using them.

APPENDIX.—REFERENCES

11. Chander, S., Spolia, S. K., and Kumar, A., "Flood Frequency Analysis by Power Transformation," *Journal of the Hydraulics Division*, ASCE, Vol. 104, No. HY11, Proc. Paper 14179, Nov., 1978, pp. 1495–1504.
12. Gupta, V. L., "Selection of Frequency Distribution Model," *Water Resources Research*, Vol. 6, 1970, pp. 1193–1198.
13. Jenkinson, A. F., "Estimation of Maximum Floods," *Technical Note 98*, World Meteorological Office, Chapter 5, 1969, pp. 183–257.

Discussion by Donthamsetti V. Rao,[4] M. ASCE

The author presents a new method of fitting hydrologic data by linear regression to probability distributions which are plotted as straight lines on specific probability papers. This method permits combining flood estimates from different distributions under a Bayesian framework. The writer offers the following comments.

Because the proposed fitting procedure is innovative, very little is known about its statistical properties. Thus, before advocating the method as an effective fitting procedure, there is a need to: (1) Establish its statistical properties, such as its bias and efficiency in estimating different design events; and (2) compare these properties with the traditional fitting methods of moments (MO) and maximum likelihood (ML). In Table 7, the writer presents the 100-yr design values for the author's sample by MO and ML. These results show that the author's method overestimates the design values compared to MO and ML methods, especially for the log normal and Gumbel models, where the differences are as high as 9%–25%. At present, there is no way of telling whether the author's results are an improvement over the MO and ML methods. However, since the properties of MO and ML are relatively well-known, the high disparities in the present results suggest, at best, that probably the author's method will produce biased (and thus, poor) estimates of design values for most models.

The author makes an understatement by saying "the Monte Carlo simulation studies assume the existence of a known probability distribution in the real world." Monte Carlo simulation is a powerful technique available with the advent of digital computers to systematically study several properties of the data samples and fitting methods of a random variable; such properties are ordinarily not tractable mathematically. This technique, e.g., is the only means available to study the properties of the author's proposed fitting method. With regard to the relevance of the Monte Carlo simulation to a real world situation, if samples from several theoretic distributions exhibit similar properties, such as that the sample skew of a small size sample is an underestimate of the population skew (19) or that the ML estimates of design values are less variable than by other methods, it is reasonable to believe that the samples from the unknown distribution of the real world also will behave accordingly.

Finally, the concept that each model could be potentially correct may not be acceptable at this time. Historically, many methods were evolved and used

[3]July, 1980, by Wilson H. Tang (Proc. Paper 15532).
[4]Hydro., St. Johns River Water Management Dist., P.O. Box 1429, Palatka, Fla. 32077.

to derive flood magnitude-frequency relations (15,17). In the course of time, several methods were discontinued and others had varying degrees of popular acceptance. A possible reason as to why each of several distributions had strong proponents among hydrologists in the past, is that in a humid area where flows are less variable, all methods gave results that are generally satisfactory (16). Also, some agencies chose a particular model and continued to use it either for consistency or due to a certain theoretic appeal of the models (i.e., Gumbel by the United States Weather Bureau, now the National Oceanic and Atmospheric Administration and log normal by the United States Army Corps of Engineers). Eventually, as more data became available from many stream gaging stations, studies were conducted to compare the results given by different models in a general fashion (14,16); such studies indicate that some models give inaccurate (i.e., unsatisfactory) results under certain conditions. For a given hydrologic sample, by reasoning, several models could be eliminated as unfit as follows.

Two basic attributes of a probability model are: (1) The distribution of probabilities of the random variable, i.e., how the cumulative distribution function plots on a reference probability paper, like normal or log normal; and (2) the statistical parameters, SP, of the random variable, such as mean, $\bar{Q}$, variance,

TABLE 7.—Predicted Design Values by Methods of Moments and Maximum Likelihood, in cubic feet per second

Model (1)	Data from 1959–1975		Data from 1959–1977	
	MO method (2)	ML method (3)	MO method (4)	ML method (5)
Normal	6,780	6,780	6,540	6,540
Log Normal	8,700	8,440	8,410	7,860
Gumbel	8,130	7,250	7,840	6,820

Note: 1 cfs = 0.028 m^3/s.

S_Q^2, and the coefficient of skewness, CS. For the real world data, the cumulative distribution function is not known; however the estimates of SP can be obtained from sample data. Even though these estimates could be biased, especially that of CS, they still provide qualitative information about the real world random variable. For the 1959–1975 and 1959–1977 data of Salt Fork (author's sample), the conventional unbiased estimates of skewness are: CS = 1.354 and 1.511, respectively, for data in real space, and CS = 0.193 and 0.379, respectively, for data in log space. Since the size of the samples is small, these values may be regarded as underestimates of population values. On the basis of these estimates, none of the models selected by the author is valid; for validity the normal distribution requires CS = 0 in real space, the log normal distribution requires CS = 0 in log space, and the Gumbel distribution requires CS = 1.14 in real space. The design values predicted by the three models differed greatly by the MO and ML methods (see Table 7), as well as by the author's fitting method (see Tables 2 and 5 of the original paper) because erroneous models were selected. The alternative models are three-parameter probability distributions (18).

As described in Ref. 18, by the MO method (using the CS values in real

space mentioned in the foregoing and other SP), the writer evaluated the 100-yr design values by four three-parameter models, i.e., log normal, Weibull, Pearson type III, and log Pearson type III. The results obtained by these four models are: (1) 8,290 cfs, 8,290 cfs, 8,300 cfs, and 8,320 cfs, respectively for 1959–1975 data (1 cfs = 0.028 m^3/s); and (2) 8,130 cfs, 8,160 cfs, 8,160 cfs, and 8,160 cfs, respectively for 1959–1977 data. Thus, the four models produce practically equivalent results. Probably, the author's fitting method will also lead to similar results. However, the author's method is rather tedious since for each CS value a separate probability paper has to be designed in the case of a three-parameter model. The writer's choice of the four models shows that under an appropriate choice of models, the model uncertainty is greatly reduced.

In summary, the author's fitting procedure needs an investigation for its statistical estimation properties. The severe model uncertainty portrayed by the author is the result of an erroneous choice of models; under an appropriate choice of models all models might produce practically equivalent results, in which case the Bayesian approach is ineffective in its intended purpose.

Appendix.—References

14. Beard, L. R., *Flood Flow Frequency Techniques*, Center for Research in Water Resources, The University of Texas at Austin, Austin, Tex., 1974.
15. Benson, M. A., *Evolution of Methods for Evaluating the Occurence of Floods, Water Supply Paper 1580-A*, United States Geological Survey, 1962.
16. Cruf, R. W., and Rantz, S. E., *A Comparison of Methods Used in Flood—Frequency Studies for Coastal Basins in California, Water Supply Paper 1580-E*, United States Geological Survey, 1965.
17. Jarvis, C. S., et al., *Floods in the United States, Magnitudes and Frequency, Water Supply Paper 771*, United States Geological Survey, 1936.
18. Rao, D. V., "Three-Parameter Probability Distributions," *Journal of the Hydraulics Division*, ASCE, Vol. 107, No. HY3, Proc. Paper 16124, Mar., 1981, pp. 339–358.
19. Wallis, J. R., Matalas, N. C., and Slack, J. R., "Just a Moment!," *Water Resources Research*, Vol. 10, No. 2, Apr., 1974, pp. 211–219.

Improved Stability of Dronkers' Tidal Schemes[a]

Errata

The following corrections should be made to the original paper:

Page 1366, Eq. 2*b*: Should read $\frac{2Q^{\frac{2n+1}{2m+1}}}{A^{\frac{2n+1}{2m+1}}}$ instead of $\frac{2Q\frac{2n+1}{2m+1}}{A^{\frac{2n+1}{2m+1}}}$

[a]August, 1980, by Guus S. Stelling (Proc. Paper 15660).

GEOMETRY OF GRAVEL STREAMS[a]

Discussion by Timothy R. H. Davies[2]

The author makes the reasonable assumption that self-adjustment of a gravel-bed stream takes place in response to independently-determined values of water flow rate, Q, and sediment transport rate, G_s. The sediment transport rate is then related to the bed shear stress, τ, in the channel.

Bagnold (24,25) has shown that G_s correlates extremely well with stream power γQS. The author has himself used this relationship previously (3).

If γQS is thus closely related to G_s, which is independently determined, it is clear that γQS is not free to be minimized as the author hypothesizes. The writer would appreciate the author's comments on this point, which is relevant to much of the author's previous work (3,4,5).

APPENDIX.—REFERENCES

24. Bagnold, R. A., "An Approach to the Sediment Transport Problem from General Physics," *Professional Paper 422-I*, United States Geological Survey, Washington, D.C., 1966.
25. Bagnold, R. A., "Bedload Transport by Natural Rivers," *Water Resources Research*, Vol. 13, No. 2, Apr., 1977, pp. 303–312.

MINIMUM STREAM POWER: THEORY[b]

Discussion by Timothy R. H. Davies[3] and Alex J. Sutherland[4]

The quantitative credibility of the minimum stream-power hypothesis depends in part on the second author's (16) use of measured data to support his proposition that unit stream power, $\bar{V}s$, is minimized in alluvial channels. In the present paper the authors claim that this is a special case of minimizing γQs. Guy, Rathbun, and Richardson (23) and Maddock (25) infer that the flume data used

[a]September, 1980, by Howard H. Chang (Proc. Paper 15678).
[2]Sr. Lect., Dept. of Agr. Engrg., Lincoln Coll., Univ. of Canterbury, Canterbury, New Zealand.
[b]September, 1980, by Charles C. S. Song and Chih Ted Yang (Proc. Paper 15691).
[3]Sr. Lect., Dept. of Agr. Engrg., Lincoln Coll., Univ. of Canterbury, Canterbury, New Zealand.
[4]Reader, Dept. of Civ. Engrg., Univ. of Canterbury, Christchurch, New Zealand.

by Yang (16) to support his proposition was acquired under conditions in which either the discharge, Q, and the water depth, d, were preselected and thus independent variables, or Q and the energy slope, s, were preselected. Sediment and fluid properties were also constant within a given set. The river data used presumably described short-term (periods of days or weeks) variations under conditions of constant Q and s.

Under each of these two sets of conditions, or constraints, the hypothesis of minimum γQs seems to be questionable. If Q and s are independent variables, then the value of γQs is imposed externally and cannot be minimized by adjustment of the dependent variables. With Q and d independent, Raichlen and Kennedy (28) and Mantz (26,27) have reported progress towards equilibrium in laboratory channels with initially-plane beds. In each case, the bed shear stress, and thus, energy slope and stream power, increased monotonically as equilibrium was approached. Thus, in achieving its equilibrium value of stream power, the system passed through states of lower stream power, in each of which the imposed constraints on Q and d were satisfied. It does not seem reasonable that channel development ceased as a result of stream power minimization.

A third set of constraints may be that Q and the sediment transport rate, G, are imposed on the system, as in the long-term development of natural streams. In this case, minimization of γQs implies minimization of s, since Q is imposed. If G is a single-valued function of shear stress (29), then γds is fixed, and minimization of s implies that d is a maximum. The equilibrium would occur, under the minimum stream power hypothesis, at a maximum value of depth, d. Alternatively, if G is considered to be a function of stream power (19,20), then with G fixed, the stream power is fixed and no minimization is possible. A possible variation of stream width, b, does not affect this argument, since b is a function of Q (24), and is thus not a variable when Q is independent.

An alternative hypothesis proposed by the writers (22) is that a self-formed stream achieves equilibrium when its resistance coefficient f, given by

$$f = \frac{2gds}{\bar{V}^2} = 2g\frac{b^2 d^3 s}{Q^2} \quad \ldots\ldots\ldots\ldots\ldots\ldots\ldots\ldots\ldots\ldots\ldots\ldots \quad (29)$$

is a local maximum. Examples from a variety of alluvial channel situations were cited in support of this view; Ref. 21 also lends weight to this.

Considering the third set of constraints with Q and G independent, maximizing f implies maximizing $d^3 s$. If G depends on shear stress, then ds is given and thus, d is maximized and s minimized. This is in agreement with minimizing γQs under these constraints. If, however, G depends on γQs, then s is fixed and maximizing f implies maximizing d; thus maximizing f gives a reasonable result here, whereas minimization of γQs could not occur.

With Q and d independent, maximizing f implies maximizing s and bed shear stress. This is compatible with the increases in shear stress reported (26,27,28) as flume experiments approach equilibrium, whereas the application of minimum stream power to this case requires explanation.

With Q and s independent, maximizing f implies maximizing d. This agrees with the behavior of lower-regime bed forms (21), whereas γQs cannot be minimized under these constraints.

The hypothesis of maximum f thus appears to be more widely applicable, and in some cases more realistic than that of minimum γQs.

Appendix.—References

19. Bagnold, R. A., "An Approach to the Sediment Transport Problem from General Physics," *Professional Paper 422-I*, United States Geological Survey, Washington, D.C., 1966.
20. Bagnold, R. A., "Bed Load Transport by Natural Rivers," *Water Resources Research*, Vol. 13, No. 2, Apr., 1977, pp. 303–312.
21. Davies, T. R. H., "Bedform Spacing and Flow Resistance," *Journal of the Hydraulics Division*, ASCE, Vol. 106, No. HY3, Proc. Paper 15258, Mar., 1980, pp. 423–433.
22. Davies, T. R. H., and Sutherland, A. J., "Resistance to Flow Past Deformable Boundaries," *Earth Surface Processes*, Vol. 5, 1980, pp. 175–179.
23. Guy, H. P., Rathbun, R. E., and Richardson, E. V., "Recirculation and Sand-Feed Type Flume Experiments," *Journal of the Hydraulics Division*, ASCE, Vol. 93, No. HY5, Proc. Paper 5428, Sept., 1967, pp. 97–114.
24. Leopold, L. B., Wolman, M. G., and Miller, J. P., *Fluvial Processes in Geomorphology*, W. H. Freeman & Co., San Francisco, Calif., 1964.
25. Maddock, T., discussion of "Recirculation and Sand-Feed Type Flume Experiments," *Journal of the Hydraulics Division*, ASCE, Vol. 94, No. HY4, Proc. Paper 6015, July, 1968, pp. 1139–1147.
26. Mantz, P. A., "Bedforms Produced by Fine, Cohesionless, Granular and Flakey Sediments," *Sedimentology*, Vol. 25, 1978, pp. 83–103.
27. Mantz, P. A., "Laboratory Flume Experiments on the Transport of Cohesionless Silica Silts by Water Streams," *Proceedings*, Institution of Civil Engineers, Vol. 69, Part 2, Dec., 1980, pp. 977–994.
28. Raichlen, F., and Kennedy, J. F., "The Growth of Sediment Bed Forms From An Initially Flattenned Bed," *Proceedings, Paper 3.7*, Eleventh International Association for Hydraulic Research Congress, Sept., 1965.
29. Vanoni, V. A., ed., *Sedimentation Engineering*, ASCE, New York, N.Y., 1975.

Technical Papers

Original papers should be submitted in triplicate to the Manager of Technical and Professional Publications, ASCE, 345 East 47th Street, New York, N.Y. 10017. Authors must indicate the Technical Division or Council, Technical Committee, Subcommittee, and Task Committee (if any) to which the paper should be referred. Those who are planning to submit material will expedite the review and publication procedures by complying with the following basic requirements:

1. Titles must have a length not exceeding 50 characters and spaces.

2. The manuscript (an original ribbon copy and two duplicate copies) should be double-spaced on one side of 8-1/2-in. (220-mm) by 11-in. (280-mm) paper. Three copies of all figures and tables must be included.

3. Generally, the maximum length of a paper is 10,000 word-equivalents. As an *approximation*, each full manuscript page of text, tables or figures is the equivalent of 300 words. If a particular subject cannot be adequately presented within the 10,000-word limit, the paper should be accompanied by a rationale for the overlength. This will permit rapid review and approval by the Division or Council Publications and Executive Committees and the Society's Committee on Publications. Valuable contributions to the Society's publications are not intended to be discouraged by this procedure.

4. The author's full name, Society membership grade, and a footnote stating present employment must appear on the first page of the paper. Authors need not be Society members.

5. All mathematics must be typewritten and special symbols must be identified properly. The letter symbols used should be defined where they first appear, in figures, tables, or text, and arranged alphabetically in an appendix at the end of the paper titled Appendix.—Notation.

6. Standard definitions and symbols should be used. Reference should be made to the lists published by the American National Standards Institute and to the *Authors' Guide to the Publications of ASCE*.

7. Figures should be drawn in black ink, at a size that, with a 50% reduction, would have a published width in the *Journals* of from 3 in. (76 mm) to 4-1/2 in. (110 mm). The lettering must be legible at the reduced size. Photographs should be submitted as glossy prints. Explanations and descriptions must be placed in text rather than within the figure.

8. Tables should be typed (an original ribbon copy and two duplicates) on one side of 8-1/2-in. (220-mm) by 11-in. (280-mm) paper. An explanation of each table must appear in the text.

9. References cited in text should be arranged in alphabetical order in an appendix at the end of the paper, or preceding the Appendix.—Notation, as an Appendix.—References.

10. A list of key words and an information retrieval abstract of 175 words should be provided with each paper.

11. A summary of approximately 40 words must accompany the paper.

12. A set of conclusions must end the paper.

13. Dual units, i.e., U.S. Customary followed by SI (International System) units in parentheses, should be used throughout the paper.

14. A practical applications section should be included also, if appropriate.